NASA CR-145047

THE SPECTRAL PROPERTIES OF URANIUM HEXAFLUORIDE AND ITS THERMAL DECOMPOSITION PRODUCTS

By

Nicholas L. Krascella

Prepared under Contract No. NAS1-13291
Modification No. 2

By

UNITED TECHNOLOGIES RESEARCH CENTER
East Hartford, Ct

for

NASA
National Aeronautics and
Space Administration

76-09-88-3

UNITED TECHNOLOGIES RESEARCH CENTER

UNITED TECHNOLOGIES

East Hartford, Connecticut 06108

Report R76-912208

The Spectral Properties of Uranium Hexafluoride and Its Thermal Decomposition Products

Prepared Under Contract NAS1-13291,.
Modification No. 2

REPORTED BY Nicholas L. Krascella
Nicholas L. Krascella

APPROVED BY R. L. O'Brien
R. L. O'Brien

DATE September 1976

NO. OF PAGES 71

COPY NO. _____

FOREWORD

An analytical and experimental research program on plasma core reactor technology was conducted by United Technologies Research Center (UTRC) under Contract NAS1-13291 with the National Aeronautics and Space Administration (NASA) Langley Research Center. The Technical Monitor of the Contract for NASA during the Contract period was Dr. F. Hohl. The Technical Program Manager for UTRC during the Contract period was Mr. T. S. Latham. The following three reports comprise the required Final Technical Report under the Contract:

1. Rodgers, R. J., T. S. Latham, and N. L. Krascella: Investigation of Applications for High-Power, Self-Critical Fissioning Uranium Plasma Reactors. United Technologies Research Center Report R76-912204, September 1976.

2. Roman, W. C.: Laboratory-Scale Uranium RF Plasma Confinement Experiments. United Technologies Research Center Report R76-912205, September 1976.

3. Krascella, N. L.: The Spectral Properties of Uranium Hexafluoride and Its Thermal Decomposition Products. United Technologies Research Center Report R76-912208, September 1976. (Present Report)

Report R76-912208

The Spectral Properties of Uranium Hexafluoride and Its Thermal Decomposition Products

TABLE OF CONTENTS

Report R76-912208

The Spectral Properties of Uranium Hexafluoride and Its Thermal Decomposition Products

SUMMARY

The current investigation was initiated to provide basic spectral data for gases of interest to the plasma core reactor (PCR) concept.

An experimental study was conducted to provide data with respect to the attenuation of vacuum ultraviolet (VUV) radiation by helium at pressures up to 20 atm over path lengths of about 61 cm and in the approximate wavelength range between 80 and 300 nm. These data are required to assess the possible utilization of helium as a transparent purge gas in the optical path through the reflector-moderator of an experimental, high pressure, fissioning gaseous uranium hexafluoride (UF_6) reactor and a vacuum ultraviolet spectrometer. The spectral measurements in the reactor experiment will be undertaken to determine the VUV emission characteristics of fissioning UF_6 gas and uranium plasmas and to determine the extent of nonequilibrium emission due to deposition of fission fragment energy in the gaseous nuclear fuel.

Similarly, measurements were conducted to provide basic VUV special data (currently unavailable in the literature) with respect to UF_6 and UF_6/argon mixtures in the wavelength range between 80 and 120 nm. These data are required for theoretical analysis of radiation transport in the buffer gas region of a PCR. These results would also provide baseline data for subsequent investigation of fission-fragment induced nonequilibrium radiation effects in the VUV spectral region in future planned gaseous UF_6 cavity reactor experiments.

Finally, an investigation was initiated to provide basic spectral emission and absorption data for UF_6 and possible thermal decomposition products of UF_6 at elevated temperatures. Absorption results are needed as prerequisites for subsequent theoretical analysis of radiation transport in the nuclear fuel buffer gas regions of a PCR. In addition, the relative emission results would provide a baseline for comparison of similar results generated in a theoretical radiation transport analysis. Current absorption data available in the open literature do not cover the spectral region at wavelengths greater than approximately 400 nm.

Transmission measurements were made in helium contained in a 61-cm-long cell in the wavelength range between 60 and 300 nm. Gas pressures were varied from a few tenths of an atmosphere to about 20 atm. Spectral data were obtained for standard tank gas as received and over limited spectral regions for helium which was partially purified by passing the helium through a liquid-nitrogen-cooled zeolite trap. The trap served to remove trace quantities of impurities normally found in helium. Similar measurements were made in argon at a wavelength range between 80 and 120 nm to provide baseline data for subsequent measurements in UF_6/argon mixtures. The argon tests were conducted in a 61 cm cell at pressures up to approximately 3 atm. No attempts were made to remove trace contaminants from the argon.

The transmission properties of UF_6 diluted with argon were measured in a 1.91-cm-long cell over a range of UF_6/argon partial pressure ratios from 7×10^{-3} to 5.5×10^{-2} and in the wavelength range between 80 and 200 nm. Subsequently, the transmission results were used to determine the spectral absorption cross sections of UF_6 over the wavelength range between 80 and 120 nm.

Relative emission measurements were made in hot UF_6/argon mixtures heated in a plasma torch over a range of temperatures from 800 to 3600 K. Spectral scans were made over the wavelength range from 80 to 600 nm. Emission measurements were made for mass flow ratios (UF_6/argon) of 1×10^{-3} to 8×10^{-2}. Although most emission results were recorded at total plasma pressures of 1.0 atm, a series of experiments was performed at a number of total pressures up to 1.7 atm to examine the effect of increased pressure on emission by UF_6 and/or its thermal decomposition products.

Absorption measurements were made using a tungsten-halogen lamp as a radiation source in the visible region at wavelengths from approximately 420 to 580 nm. Temperatures for these determinations were varied from about 1000 to 1800 K. All absorption measurements were at a total pressure of 1.0 atm and for a range of mass flow ratios (UF_6/argon) from 6.8×10^{-2} to 1.2×10^{-1}.

In general, the results show that relatively little emission occurs at wavelengths below about 300 nm over the temperature range investigated. At higher temperatures ($T \geq 1800$ K) very weak emission was observed between 250 and 300 nm. The total of integrated emission in the wavelength region between 300 and 580 nm increases about nine orders of magnitude as the temperature is increased from about 800 to 3600 K. A new emission band having a wavelength peak of approximately 310 nm is observed to appear at a temperature of about 1800 K; this band becomes more well defined at higher temperatures. Essentially no pressure effect was observed on the emission spectra for pressures up to 1.7 atm.

The "effective" cross sections for absorption at temperatures between 1000 and 1800 K and at wavelengths in the region between 420 and 580 nm were determined from transmission measurements. The cross sections ranged in value from about 8×10^{-19} to 9×10^{-10} cm^2 per molecule of UF_6.

The experimental spectral investigations described herein were conducted under Contract NAS1-13291 and Contract NAS1-13291, Mod. 2 with the Langley Research Center of the National Aeronautics and Space Administration. The main body of the report is concerned with recently completed investigations of the spectral emission and absorption properties of UF_6 and its decomposition products at elevated temperatures conducted under Contract NAS1-13291, Mod. 2. Investigations concerning the VUV spectral characteristics of UF_6/argon mixtures and the transmission of VUV radiation by helium at high pressures and over long path lengths was completed under Contract NAS1-13291. The latter results were published as NASA Contractor Report NASA CR-2666 and are enclosed as APPENDIX A of the current report.

INTRODUCTION

Extensive experimental and theoretical research has been conducted with respect to various aspects of fissioning gaseous uranium plasmas over the past two decades. These studies have been generally directed toward high performance nuclear space propulsion systems (Ref. 1). In addition to space applications, the PCR concept has been recognized as a possible candidate energy source for various terrestrial applications (Ref. 2). The very high operating temperatures generated by fissioning plasmas tend to enhance efficiencies of various thermodynamic cycles compared to conventional power generating systems or nuclear reactors with solid fuel elements. Furthermore, the high operating temperatures associated with gaseous fissioning reactors provide a source of very intense electromagnetic radiation with a number of possible applications involving direct coupling of energy by radiative processes.

Although most of the applications of the PCR require extensive basic research and technological development, the potential benefits from the use of these devices warrant continued investigation of the concept. Possible PCR space and/or terrestrial applications are:

(1) High-thrust, high-specific-impulse space propulsion systems.

(2) Advanced high-temperature, closed-cycle gas turbine electrical power generation.

(3) MHD conversion systems for electrical power generation.

(4) Photochemical and/or thermochemical processing.

(5) Direct pumping of lasers by deposition of fission fragment energy in UF_6 or other lasing gas mixtures.

(6) Optical pumping of lasers by thermal and/or nonequilibrium radiation emitted by a gaseous fissioning UF_6 or uranium plasma.

A typical unit cavity of a PCR device is illustrated in Fig. 1. In the PCR concept a high-temperature, high-pressure plasma is sustained via the fission process in a uranium gas injected as UF_6 or other uranium compound. Containment of the plasma is accomplished fluid-mechanically by means of an argon-driven vortex which also serves to thermally isolate the hot fissioning gases from the surrounding wall.

For applications which employ thermal radiation emitted from the plasma, an internally-cooled transparent wall can be employed to isolate the nuclear fuel, fission fragments, and argon in a closed-circuit flow loop and permit transfer of the radiant energy from the plasma to an external working fluid. For applications

which employ fission-fragment-induced short wavelength nonequilibrium radiation emitted from the plasma, the working fluid such as lasing gases can be either mixed with fissioning gas or injected into the peripheral buffer gas region such that there is no blockage of radiation due to the intrinsic absorption characteristics of transparent materials at short wavelengths.

Three fundamental areas of research are required to demonstrate the feasibility of the PCR concept: (1) nuclear criticality; (2) fluid mechanical confinement; and, (3) transfer of energy by radiation processes. Various aspects of these areas of technology are currently being investigated at UTRC. In addition, cavity reactor experiments which employ gaseous UF_6 are currently being performed at Los Alamos Scientific Laboratory (LASL) as part of the planned NASA program to determine the feasibility of PCR's.

The present report summarizes recent results of emission and absorption measurements in hot UF_6/argon mixtures at various wavelengths, temperatures, and pressures. These data are required to provide basic absorption data for radiation transport calculations and relative emission data for subsequent comparison of theoretical calculations with experimental results.

TEST EQUIPMENT

A description of the equipment used in the determination of the VUV transmission properties of high pressure helium and UF_6 are described in APPENDIX A.

The equipment used in the experimental evaluation of the spectral properties of UF_6 and possible UF_6 decomposition product consisted of three major components. These were the plasma torch-optical plenum assembly, the monochromator, and the UF_6 transfer system. A schematic of the overall system is shown in Fig. 2; details of these components as well as other auxiliary equipment are discussed in the following sections.

Plasma Torch-Plenum Assembly

A plasma torch facility, designed and developed by UTRC, was used to provide hot UF_6/argon mixtures for all experimental determinations. A photograph of the torch-plenum assembly is shown in Fig. 3. A cross-sectional schematic of the plasma torch illustrating the major torch components is depicted in Fig. 4. The principal components of the torch are a pin-type cathode, a hollow conically-shaped anode, an argon injector, a UF_6 injector, and two external magnets. The cathode is a hemispherical-tipped 2 percent thoriated tungsten rod 0.1 cm in diameter and was provided with means for independent water cooling. The cathode extended partially into the water-cooled conically-shaped copper anode as shown in Fig. 4. Argon was injected tangentially through eight equally spaced 0.016-cm-diameter holes located at the base of the cathode assembly. The aerodynamic swirl imparted by the argon injection system was augmented magnetically by means of two external magnets located concentrically about the anode as shown in Fig. 4.

A Rapid Electric, Model SRV/MAN, 200 kW dc power supply was used to provide power to the discharge. The external magnets were supplied by Hypertherm Model H-444 dc power supplies rated at 16.2 kW (90 v, 180 A) with a 60 percent duty cycle. The large magnet was connected to two parallel Model H-444 supplies to provide higher current (360 A) and, thus, a greater magnetic field. The smaller magnet was supplied by one Model H-444.

A UF_6 injector was located immediately adjacent to and downstream of the anode. Preheated UF_6 was injected into the argon stream heated by the torch via two 0.016-cm-diameter holes. The aerodynamically mixed high temperature gas stream was then introduced into the cylindrical stainless-steel plenum (see Figs. 2 and 4). The plenum was equipped with six optical ports (three oppositely positioned pairs) which enabled viewing the high temperature gas stream spectroscopically in absorption or emission. The optical path through the mixed gas stream was 10.2-cm-long. The hot exhaust gases were subsequently cooled in a heat exchanger consisting of multiple copper coils prior to being neutralized in a sodium bicarbonate scrubber.

A high pressure (40 atm) water pump was used to provide cooling water for critical torch components. Separate water flow loops were used to cool the cathode, anode, external magnets and the UF_6 injector. Water cooling was not provided for the optical plenum. Each cooling water flow loop contained a flow meter to monitor water volumetric flow and a thermocouple to monitor exit water temperature. Inlet water temperature was also monitored by means of a thermocouple. Thus, power dissipation in various components could be calculated. Similarly, a flow meter was installed in the argon line to the torch to provide means for quantitatively measuring argon mass flows in the system. Three thermocouples were attached to the plenum to monitor wall temperatures in the vicinity of the optical ports as shown in Fig. 4. A fixed thermocouple was inserted into the hot gas flow downstream of the plenum and immediately prior to the heat exchanger. In addition, a scanning thermocouple system (tungsten - 5 percent, rhenium vs. tungsten - 26 percent rhenium thermocouple) was installed such that temperature scans could be made in the UF_6/argon mixture parallel to the optical path.

The plenum was equipped with both a transducer and a gauge for monitoring total pressure in the system. All thermocouples associated with monitoring water, component, and exit-gas temperatures were copper-constantan. Temperatures were monitored by means of an eight channel Sanborn recorder.

Monochromator

A McPherson Model 235, half-meter scanning monochromator was used for all spectral measurements. The monochromator was of the Seya-Namioka-type. Entrance and exit slit systems contained three slit widths; 100, 200, and 400 μm. A 1200 L/mm and a 300 L/mm grating were available for use. The 1200 L/mm grating was blazed at 150 nm and covered the range from 50 to about 300 nm. The 300 L/mm grating was blazed at 550 nm and covered a wavelength range from 50 nm to about 1200 nm. Scanning speeds could be varied in twelve steps from 0.025 nm/minute to 100 nm/minute for the 1200 L/mm grating and from 0.1 nm/minute to 400 nm/minute for the 300 L/mm grating.

The radiation detector system consisted of a McPherson Model 650 detector assembly and a Model 790 detector electronic system. The detector contains a sodium salicylate coated window and an EMI Model 9635B "dialkali" coated photomultiplier. The sodium salicylate-photomultiplier system is sensitive from 50 to about 600 nm. The 600 nm upper wavelength limit is dictated by the photomultiplier cutoff. The detector output was monitored on one channel of a Hewlett-Packard dual channel recorder.

A 2.5 cm diameter transition section approximately 30 cm in length was used to provide an enclosed optical path between the plenum and the monochromator. The end of the transition piece in contact with the inner wall of the plenum was fitted with a 0.6 x 1.9 cm slit to minimize flow of UF_6 into the external optical path. The transition section was equipped with a window mount to permit use of a lithium fluoride window when scanning at wavelengths above approximately 120 nm. In addition, an argon purge system was installed in the transition section to provide a slight back-pressure of gas with respect to the plenum, in order to prevent flow of UF_6 from the plenum into the monochromator or onto the windows. In addition, the monochromator housing and the window assembly used in conjunction with the tungsten-halogen source lamp for absorption measurements were provided with argon purging to prevent possible contamination by UF_6 vapors.

UF_6 Transfer System

The transfer system consisted of a two liter Monel supply canister rated at 200 atm with appropriate shut-off and metering valves as indicated in Fig. 2. Two chromel-alumel thermocuples were installed in the canister to monitor the temperature of the UF_6 liquid and gas phases. A Matheson linear mass flow meter was used to determine UF_6 mass flow rates during various experiments. The mass flow meter output was continuously monitored on the second channel of the Hewlett-Packard dual channel recorder during all tests involving UF_6 flow. The canister, valves, mass flow meter, and all lines in the UF_6 transfer system were electrically heated by means of Variac controlled heater tapes. Chromel-alumel thermocouples were placed in various components to monitor temperatures at strategic locations in the UF_6 flow loop.

EXPERIMENTAL PROCEDURES

The experimental procedures and operating parameters associated with the experimental measurements of the VUV transmission of argon and UF_6 are described in APPENDIX A.

A series of preliminary experiments was conducted to establish the operating parameters of the plasma torch system and to establish cooling water flow requirements for the facility. This series of tests was conducted with argon flow only; no UF_6 was used nor were spectral scans made. Similar studies were conducted using helium as the torch gas in order to allow greater variation in the UF_6/torch gas mass-flow ratios or equivalently greater partial pressures of UF_6. However, operation of the torch on helium required substantially higher flow rates and yielded lower temperatures as compared to argon. Anode erosion also appeared to be more severe with helium as a torch gas in contrast to argon. Therefore, use of helium as a torch gas was discontinued. During these tests water flow and temperatures were monitored as well as temperatures for various system components. Similarly, gas exit temperatures were measured. In addition, these tests indicated that run time decreased markedly (about three minutes) at operating conditions which yielded temperatures above approximately 2000 K. The limiting factor with respect to operating time was primarily attributable to thermal overloading of the external magnet power supplies.

It should be noted that the flow rate of argon determines the gas-mixture temperature in the plenum to a very large degree. Thus, variation of the argon flow to obtain various UF_6-to-argon mass ratios was precluded. Changes in UF_6-to-argon mass flow were accomplished by varying the quantity of UF_6 injected into the gas stream.

Subsequently, spectral studies with flowing UF_6 were undertaken. Normal procedure involved initiating the discharge on argon injected at a low flow rate to facilitate start-up. The argon flow and discharge current were then increased to predetermined values and the system allowed to equilibrate. Spectral scans were then conducted to determine the emission from argon without UF_6 flow. Prior to starting, the UF_6 transfer system was preheated to a temperature of approximately 430 K. UF_6 was not injected until the injector temperature was greater than 350 K to prevent condensation of UF_6 in the injector ports with resultant clogging of the UF_6 injector system.

After the UF_6 injector reached operating temperature, UF_6 flow was initiated and monitored by means of the linear mass flow meter until constant flow was obtained. Constant UF_6 flow usually was achieved between 30 to 60 seconds after flow was initiated. Spectral scans in either emission or absorption were commenced after equilibration of UF_6 mass flow.

Temperature scans were taken immediately after the spectral scans were completed. The temperature and spectral scans were not conducted simultaneously because of objectionable photodetector noise levels generated by the scanning thermocouple drive-motor.

Spectral data were recorded at a rate of 400 nm/minute when using the 300 L/mm grating and at 100 nm/minute when using the 1200 L/mm grating. The high scan rates were required because of relatively short plasma torch operating times at high temperatures and to minimize exposure of the equipment to hot corrosive UF_6. Monochromator slit width was constant at 100 μm for all emission and absorption measurements.

Initial spectral results were of poor quality because of high noise levels. The problem was traced to a low frequency (several cps) vibration introduced into the plasma torch - monochromator system by a large vacuum pump operating adjacent to the plasma torch facility. Subsequently, the monochromator table was equipped with "isopads" and additional mounting support provided for the plasma torch plenum assembly. In addition, a metallic bellows was installed in the transition section between the plenum port and the monochromator entrance slit to minimize vibrational coupling between the two systems. With these changes the vibration was reduced to negligible levels.

A tungsten-halogen lamp (quartz envelope) was used as the radiation source for the absorption measurements. Initially a high-speed chopper ($\sim$660 cps) was installed to discriminate between lamp radiation and UF_6 emission. The mechanical vibrations previously discussed were markedly amplified by the phase-sensitive system. As a result, spectral traces obtained using phase-sensitive detection were unusable. Attempts to further isolate the equipment were not successful and the phase-sensitive detector scheme for absorption studies was abandoned. Therefore, absorption measurements were conducted as follows. First, a spectral scan was made at a given argon mass flow rate and gas temperature to determine the emission due to hot argon. In all cases investigated no argon emission could be observed except under very high amplifier gain as compared to the lamp or UF_6 emission. Consequently, the incident radiation, I_o, was measured by irradiating the hot argon with the lamp at the specified operating conditions. Next, a UF_6 flow was established and the combined radiation, $I_{UF_6} + I_t$, (from the lamp and UF_6 emission) was measured. This measurement gives the total radiation emitted by the hot UF_6 and the quantity of lamp radiation which is transmitted through the plasma. Finally, the emission due to UF_6, i.e., I_{UF_6}, was determined with the lamp extinguished. Thus, the relative intensity transmitted through the absorbing plasma was determined and is given by:

$$\frac{(I_{UF_6} + I_t) - I_{UF_6}}{I_o} = \frac{I_t}{I_o} \qquad (1)$$

Shutdown procedure involved termination of UF_6 flow followed by careful purging of UF_6 transfer lines and the UF_6 injector system with argon preheated to a temperature of approximately 500 K. Failure to adequately purge the system with hot argon invariably resulted in condensation of UF_6 upon cooling and complete clogging of the small ports in the UF_6 injector.

Wavelength calibration of the two gratings was periodically effected using a mercury discharge lamp placed at the entrance slit to the monochromator.

Periodic post-test examination of various components such as the anode, cathode, and plenum was made to determine possible effects of UF_6 corrosion on these components. Samples of component deposits containing uranium were acquired and analyzed. Similarly, the lithium fluoride windows used in most experiments underwent post-test visual examination for deposits which might degrade transmission characteristics. In addition, transmission characteristics of the lithium fluoride windows were checked for degradation by determining the relative transmission before and after exposure to UF_6 using the tungsten-halogen or Hg lamps as a reference radiation source. Under no conditions were the window transmissions found to be degraded due to uranium compound deposits.

The linear mass flow meter incorporated as part of the UF_6 transfer system functioned very well during early experiments. However, after approximately 800 to 1000 g of UF_6 had been used in the system, a marked deterioration in output (voltage) as a function of flow rate (g/s) occurred. The sensor head was examined and found to be coated with a grey deposit which was partially removed by flushing with acetone. Reassembly and calibration with argon as a flow medium revealed a change in the meter voltage output as a function of mass flow. Therefore, an argon flow system was installed to permit periodic on-line calibration of the flow device. Suspect emission results (erroneous UF_6 flow rates) obtained during this period comprised approximately seven scans which were discarded and are not reported herein.

RESULTS AND DISCUSSION

The experimental results with respect to the VUV transmission properties of helium and UF_6 are summarized in APPENDIX A. The following paragraphs summarize the spectral results obtained with respect to the high temperature emission and absorption characteristics of UF_6 and possible UF_6 thermal decomposition products.

Relative Spectral Emission

A series of twenty-six separate emission scans were made for wavelengths in the region between 120 to 600 nm. The 300 L/mm grating was used for these studies along with the lithium fluoride window. The window was utilized primarily to eliminate the possible contamination of the monochromator components by UF_6.

Experimental parameters including temperature, UF_6 and argon mass flow rates, the calculated partial pressure of UF_6, and the UF_6-to-argon mass flow ratio are summarized in TABLE I for these twenty-six runs. The pressure in the optical plenum was maintained at 1.0 atm for all twenty-six cases described in TABLE I.

It should be noted that the maximum range for a sheathed tungsten thermocouple is approximately 3000 K. Therefore, the value of 3560 K (scan number 26) represents the result of three temperature estimates. These are: (1) an extrapolation of the thermocouple calibration curve to higher temperatures; (2) heat balance for the system which defines an average gas temperature; and, (3) a correlation between observed temperature profiles (obtained with the scanning thermocouple) and an average gas temperature as determined by the thermocouple in the partially cooled gas stream well downstream of the optical path.

Three representative gas-mixture (UF_6/argon) temperature profiles are shown in Fig. 5 as a function of relative position along the optical path in the plenum immediately adjacent to the UF_6 injector. The profiles are relatively flat usually exhibiting a maximum temperature variation of less than approximately 100 K. Since a relatively large thermocouple was used (0.32-cm-dia), the steep temperature gradient adjacent to the walls of the optical plenum are not evident in Fig. 5. Wall temperatures measured at the outer surface of the plenum ranged from 800 to about 1500 K and depended essentially upon the argon flow rate and the run duration. There was no direct correlation between wall temperatures and gas temperature since spectral scans were initiated as soon as possible to reduce run time and exposure to UF_6. In essence, equilibrium between the gas-mixture and wall temperature was not necessarily established prior to spectral scanning. The effect of this thermal nonequilibrium of the walls on spectral scans was negligible as noted on repetitive spectral scans at nearly identical gas temperatures but different wall temperatures.

Results of typical emission scans are illustrated in Fig. 6 as a function of wavelength for several temperatures between approximately 1000 K and 3600 K. The relative intensities shown in Fig. 6 have been corrected for various variable experimental parameters such as photodetector response and different scale factors. The emission due to argon was always found to be negligible compared to UF_6, thus no correction for argon emission was required. In addition, the measured relative emission intensities have been normalized by dividing the corrected intensities by the corresponding calculated partial pressure of UF_6. Therefore, these results illustrate the emitted intensities per unit pressure (mm Hg) of UF_6 injected into the system.

The long wavelength limit or cutoff (580 nm) was dictated by the photodetector response which rapidly approached zero between 580 and 600 nm. In all cases experimentally investigated, the emitted intensity from hot UF_6 reached negligible levels between 250 and 300 nm. This result was not unexpected since a black-body at a temperature of 3560 K radiates only 5.6×10^{-2} perecent of its energy at wavelengths less than 30 nm.

All spectral traces shown in Fig. 6 exhibit similar characteristics, particularly in the visible region between 380 and 580 nm. The first appearance of a new emission band at a wavelength of about 310 nm is noted at about 1800 K and becomes more pronounced with increasing temperature. In addition, there is an enhancement in emission at wavelengths less than about 380 nm with an increase in temperature.

The spectral emission results of Fig. 6 were integrated between 300 and 580 nm to determine the variation in relative total emission as a function of temperature. These calculated total emission results are depicted in Fig. 7 as a function of temperature and are normalized with respect to the integrated results at 3650 K. No data below 300 nm or above 580 nm were used because of the very weak signal observed. The total intensity between 300 and 580 nm increases rapidly up to a temperature of about 1700 K and then much less strongly at higher temperatures as shown in Fig. 7. The emission increases approximately by nine orders of magnitude between 800 and 3600 K. A summary of these results and integrated intensities at lower temperatures is shown in TABLE II. Equivalent integrated black-body data over the same temperature range and in the same wavelength range are also illustrated by the dashed line in Fig. 7. The total emission from UF_6 and its possible decomposition products increases at a rate similar to that of an equivalent black-body over the same temperature range as demonstrated in Fig. 7.

Fractional integrated intensities per 40 nm wavelength intervals were calculated from the results of Fig. 7. These calculated results are shown in Fig. 8 as a function of the wavelength at the center of each 40 nm interval for four representative temperatures between 1400 and 3600 K. The results in Fig. 8 illustrate the enhanced emission at wavelengths below 400 and 450 nm as the temperature is increased and the

corresponding decrease in emission with increasing temperature at longer wavelengths. Additional calculated fractional intensities not shown in Fig. 8 are tabulated in TABLE III for all temperatures investigated.

The calculated equilibrium composition of UF_6/argon mixtures is shown in Figs. 9 and 10 as a function of temperature at a total pressure of one atmosphere (Ref. 3). The results shown in Fig. 9 were calculated for a partial pressure of UF_6 equal to 0.5 mm Hg, and in Fig. 10 for a partial pressure of UF_6 equal to 5 mm Hg. Comparison of the spectral emission results of Fig. 6 with the composition data of Figs. 9 and 10 indicate that the appearance of the new band (peak $\lambda \sim 310$ nm) occurs at about 1800 K and approximately coincides with the appearance of the UF_6 decomposition products, UF_4 and UF_5 as well as fluorine atoms, F. Assignment of the band to a specific species is not possible on the basis of these data. Further assessment of the spectral results with specific components from the thermal decomposition of UF_6 are precluded because of the complexity of the composition scheme at higher temperatures.

It is known from black-body relationships that only about 0.21 percent of the total emitted radiation occurs at wavelengths less than 300 nm for a black-body at a temperature of 3560 K. Therefore, relatively little emission of radiation was anticipated for UF_6 and/or its decomposition products at the same temperature or at lower temperatures. Although the previously described experimental results indicated no radiation below 250 nm at any temperature, a series of three emission scans were made to confirm these results and to examine the spectral region below the lithium fluoride wavelength cutoff at approximately 120 nm. These scans were accomplished in a windowless mode using the 1200 L/mm grating at temperatures of 1050, 1400, and 2280 K. Additional experimental parameters are enumerated in TABLE IV. No radiation (line, band, or continuum) was observed in confirmation of the previous results. Therefore, additional scans in the windowless mode were discontinued because of possible exposure of the slit system and grating to corrosive UF_6.

A final series of six emission studies was conducted at total plenum pressures up to 1.7 atm to examine the effect of pressure on the emission from hot UF_6 and its thermal decomposition products. The various experimental parameters for these cases are summarized in TABLE V. The result of these tests did not indicate an appreciable pressure effect as shown by a comparison of the relative spectral emissions at a temperature of about 2400 K for a total pressure of 1.0 and 1.7 atm (see Fig. 11). Similar results were obtained at other temperatures and pressures. The two curves depicted in Fig. 11 are also indicative of the reproducibility of the previous emission results at similar temperatures observed in the scans at a total pressure of 1.0 atm.

Spectral Absorption

Finally, a series of five experiments was performed to ascertain the absorption characteristics of UF_6 in the visible region and at elevated temperatures. A typical set of emission results at a temperature of 1270 K are shown in Fig. 12 as a function of wavelength between 420 and 580 nm. The figure illustrates the source intensity (tungsten-halogen lamp) I_o, the combined intensity from the emitting UF_6 plus the transmitted source intensity ($I_{UF_6} + I_t$),as well as the emissions from the hot UF_6, I_{UF_6}.

The relative spectral transmission derived from the results of Fig. 12 and similar results for other temperatures are shown in Fig. 13. These data were used to determine "effective" spectral cross sections over the wavelengths of interest as follows:

$$\frac{I_t}{I_o} = \exp(-\sigma N L) \qquad (2)$$

where I_t/I_o is the transmission (Fig. 13), N, the number density, L the path length, and σ the cross section. The quantity σ is an "effective" cross section since the UF_6 may be partially decomposed, particularly at higher temperatures. Furthermore, the individual spectral details associated with each absorbing species cannot be ascertained. Therefore, the particle density factor serves to define an "effective" cross section per unit UF_6 pressure. Calculated "effective" cross section results are graphically depicted in Fig. 14 as a function of wavelength at the temperatures studied.

The magnitude of the "effective" cross section varies from about 8×10^{-19} cm^2 at short wavelengths to a minimum of approximately 9×10^{-20} cm^2 at the long wavelengths. Tabulated values of the cross section at 10 nm intervals are summarized in TABLE VII for the five temperatures investigated.

Analytical Chemistry

Approximately eight samples of uranium compound deposits were taken from the anode assembly, UF_6 injector, UF_6 transfer lines, the plenum walls, the heat exchanger, and the teflon spacer (electrical insulator between the anode and UF_6 injector) for qualitative analysis of the uranium compounds present.

The samples were invariably grey or greenish-grey in color. The principal species present in each case was the uranyl ion, UO_2^{++}, with indications of traces of UO_3. An infrared spectrophotometric trace of a typical sample is illustrated in

Fig. 15. (UO_2^{++} peak occurs at about 10.5 μm, UO_3 peak at about 7.3 μm). Occasionally an analysis indicated the presence of UF_4 and copper fluoride, CuF_2. The CuF_2 was found in a sample obtained from the anode and the UF_6 injector assembly, both of which are made of copper. These results were in part confirmed by the solubility of the samples in water. For example, the pale grey deposits could be effectively dissolved in water indicating the presence of UF_6 or UO_2F_2, since UF_4 and UO_3 are completely insoluble by comparison. No noticeable evidence of corrosion was observed except on the anode surface. The "pitting" on the anode surface is undoubtedly due to attachment of the arc at the anode surface rather than to direct attack of the anode by hot UF_6 since relatively little UF_6 can be found upstream of the UF_6 injector.

All surfaces which are contacted by UF_6 eventually were observed to be coated with the characteristic grey or greenish-grey deposit previously described. Similarly, these deposits were almost completely water soluble, again indicating UO_2F_2. Since the plasma torch system before, during, and after operation is essentially isolated from the atmosphere, hence isolated from oxygen or water vapor, the uranyl compound cannot be attributed to thermal decomposition of UF_6. Uranyl fluoride most probably forms after disassembly of various components with consequent exposure to atmospheric water vapor or in subsequent processing for analysis in the following manner.

$$UF_6 + 2H_2O = UO_2F_2 + 4HF \qquad (3)$$

At least three samples were extracted from the gases in the plenum immediately after spectral scans in an effort to ascertain chemical constitution of the heated mixture. Sampling was accomplished by means of a 0.16-cm-ID stainless steel probe positioned at the axial center of the plenum. The probe was exhausted into an evacuated pyrex sample tube approximately 500 cm^3 in volume. The results were inconclusive in that only argon could be positively identified in the gas phase. Presence of UF_6 or some other reactive uranium compounds was indicated by very small areas of a whitish or grey-white deposit which appeared on the inner surface of the sample tubes. These deposits were in part water soluble. No additional samplings of the hot gas mixture were attempted.

CONCLUSIONS

In summary, the transmission characteristics of helium, argon, and UF_6/argon mixtures have been experimentally examined over a range of wavelengths and pressures. The helium results indicate that helium could be used as a high pressure, transparent purge gas in future fissioning plasma VUV emission studies provided trace impurities are sufficiently removed. In addition, the cross section results obtained for UF_6 in the VUV region represent the only known quantitative data available for this compound. These cross section data will be used in subsequent analytical radiation transport analyses related to performance studies of the PCR concept and experiments.

In addition, the broadband relative spectral emission characteristics of UF_6 and its thermal decomposition products have been experimentally examined over a range of wavelengths (120 to 580 nm), pressures (1.0 to 1.73 atm), and temperatures (800 to 3600 K). The "effective" absorption cross sections of UF_6 and its thermal decomposition products have been determined over the wavelength range from 420 to 580 nm and at five temperatures between approximately 1000 and 1800 K.

The following conclusions are inferred from these experimental investigations:

1. The total integrated intensity between 300 and 580 nm increases with temperature between 800 and 3600 K at approximately the same rate as a black-body at equivalent temperatures.

2. There is no significant emission of radiation at wavelengths between 80 and approximately 250 nm for the temperature region investigated.

3. The appearance of a new emission band centered at approximately 310 nm is associated with the appearance of substantial quantities of UF_6 thermal dissociation products at temperatures in excess of 1800 K.

4. The emission of radiation from UF_6 or its dissociation products does not exhibit a measurable pressure dependence at total pressures up to 1.7 atm.

REFERENCES

1. Thom, K., R. T. Schneider, and F. C. Schwenk: Physics and Potentials of Fissioning Plasmas for Space Power and Propulsion. Paper No. 74-087, International Astronautical Federation (IAF) XXVth Congress, Amsterdam, Holland, 30 September - 5 October 1974.

2. Latham, T. S., F. R. Biancardi, and R. J. Rodgers: Applications of Plasma Core Reactors to Terrestrial Energy Systems. AIAA Paper 74-1074, AIAA/SAE 10th Propulsion Conference, San Diego, CA., 21-23 October 1974.

3. Roback, R.: Thermodynamic Properties of Coolant Fluids and Particle Seeds for Gaseous Nuclear Rockets. United Aircraft Research Laboratories Report C-910092-3, September 1964, Prepared Under NASA Contract NASw-847.

SYMBOLS

L/mm	Number of lines or grooves/mm of grating surface
I	Relative transmitted intensity for absorption measurements (see Fig. 12), dimensionless
I_o, I_o'	Relative source lamp intensity or incident intensity, dimensionless
I_t	Relative transmitted intensity, dimensionless
$I_\lambda(T)$	Relative spectral emission at temperature, T, dimensionless
$I_t(T)$	Relative total or integrated emission at temperature, T, dimensionless
$I_{\Delta\lambda}(T)$	Relative integrated spectral emission per wavelength interval, dimensionless
L	Path length, cm
$\dot{m}$	Mass flow rate, g/s
N	Number density, cm^{-3}
P	Pressure, atm or mm Hg
Q	Volumetric flow rate, liter/minute at STP
r	Relative position, dimensionless
T	Absolute temperature, deg K
T'	Transmission (I/I_o x 100) or (I/I_o' x 100)
λ	Wavelength, nm or μ
σ	Cross section, cm^2 per molecule of UF_6

APPENDIX A

VACUUM ULTRAVIOLET CHARACTERISTICS OF HIGH PRESSURE HELIUM AND URANIUM HEXAFLUORIDE/ARGON MIXTURES

Test Equipment

A McPherson Model 235, half-meter scanning monochromator was used for all spectral measurements. A schematic diagram of the monochromator and accessories, gas cell and gas handling system, is shown in Fig. 16 and is photographically displayed in Fig. 17. The monochromator was of the Seya-Namioka-type and had a full aperture ratio of f/11.4. Wavelength scan rates were variable in twelve steps from 0.025 nm/minute to 100 nm/minute. A 10.2 cm, 750 ℓ/s high-speed, oil-diffusion pump and a 425 ℓ/minute Welch mechanical pump comprised the basic pumping system for the monochromator. The monochromator was equipped with a 1200 line/mm grating, blazed at 150 nm which allowed measurements in the wavelength range between 50 and 300 nm. The linear dispersion of the grating was quoted to be 1.66 nm/mm. Resolution was 0.05 nm when used with 10 μslits.

Model 820 differential slit systems were used at both the entrance and exit ports of the monochromator. Each differential slit system was equipped with slits of widths of 10, 50, and 100 μ.

A McPherson Model 630 high energy, VUV, Hinteregger-type discharge lamp was used as the source of radiation in conjunction with a Model 720 high-voltage dual-mode power supply. The source system can be operated as an air-gap controlled, high-voltage spark or as an ac arc. Only the former operating mode was used during the study since the spark mode provided enhanced continuum radiation when the lamp was charged with various rare gases. Helium, argon, and xenon were used as source gases and provided continuum radiation in the approximate wavelength range between 60 and 200 nm. The approximate useful wavelength ranges for these rare gases were:

Gas	Range-nm
Helium	60.0 - 105.0
Argon	105.0 - 145.0
Xenon	145.0 - 195.0

A simple Westinghouse tungsten-iodine lamp was used as the radiation source in the wavelength range between 200 and 300 nm.

The radiation detector system consisted of a McPherson Model 650 detector assembly and a Model 790 detector electronic system. The detector contains a sodium salicylate coated window and a Model 9514B phototube. Ultraviolet radiation incident upon the sodium salicylate causes fluorescence at about 400 nm which is subsequently detected by the photomultiplier, amplified, and recorded. Although the sodium salicylate/photomultiplier system is sensitive from 50 to 600 nm, the linear response range was from 50 to about 300 nm.

Two gas cells were designed and fabricated for the transmission measurements. Transmission measurements in high pressure helium were made in a 7.6-cm-ID, 61-cm-long stainless steel cell as shown in Fig. 16. The cell was positioned between the monochromator exit slit and the detector. Pressure transducers and thermocouples were connected to the test cell to permit pressure and temperature monitoring. Since the pumping speed is greatly attenuated through small slits, a separate mechanical vacuum pump was used to assist in evacuating the test cell as shown in Fig. 16.

Although initial experiments with UF_6/argon mixtures were attempted in the 61 cm cell, the mixtures proved to be extremely opaque and no radiation was transmitted through the 61 cm path length. A short-path-length cell was constructed of 5-cm-dia copper tubing in which the spectral transmission properties of various UF_6/argon mixtures were determined (see Fig. 18). The length of this cell was 1.91 cm. A 0.95-cm-OD inlet port with provision for a thermocouple and a 0.95-cm-OD outlet port with provision for a pressure transducer were located at the axial midpoint. The copper cylinder was soldered to two 10.2-cm-dia brass flanges which provided mounting to the exit slit and subsequent mounting of the detector housing. Initially, 1.9-cm-dia ports in each flange permitted passage of radiation through gas samples. Each flange was drilled with two inlet and exit (0.32 cm) injectors through the 0.95 cm thickness to permit injection of argon at one side of the optical aperture. Ports opposite the argon injectors were installed to allow pumping of injected argon in an attempt to prevent flow of UF_6 into the monochromator chamber and to prevent deposition or reaction of UF_6 on or with the sodium salicylate. Since the system provided marginal protection to the sodium salicylate coating, subsequent experiments were performed with one argon inlet port at the entrance to the cell and with all four ports at the cell exit also injecting argon into the cell. In addition, an insert was machined to reduce the area of sodium salicylate exposed to UF_6 and placed in the cell exit flange. An aperture, located in the insert, 0.48 cm in width and 1.59 cm in height allowed the radiation to pass through gases in the cell. In this configuration, all argon injected into the cell was pumped out through the UF_6/argon exit port located at the axial midplane of the cell proper. With this flow arrangement, no degradation of the sodium salicylate coating was observed. Similarly, no evidence of condensation of UF_6 on the monochromator exit slit system or on the grating was evident by physical inspection or by spectral monitoring before or after exposure to UF_6.

The UF_6 handling system consisted of a stainless steel UF_6 supply cylinder, a sodium fluoride (NaF) trap, and appropriate shutoff and metering valves. The NaF trap was installed to remove traces of HF usually found admixed with UF_6. Six thermocouples were installed to monitor temperatures at various strategic locations. These details are shown in Fig. 16. Argon was supplied to the system via the cell injectors previously described. All lines, the test cell, and associated equipment were electrically-heated by means of controlled heater tapes.

A zero-to-50 mm Hg Wallace and Tiernan absolute pressure gauge was used to monitor monochromator chamber pressures. Similarly, a zero-to-200 mm Hg Wallace and Tiernan absolute pressure gauge was used to monitor source-lamp gas pressures. Absolute pressure transducers of appropriate ranges were mounted on the test cells to ascertain gas pressures in the gas cells. Pressure transducer output was displayed on a recorder as well as on a vacuum tube volt meter.

The helium and argon used for the VUV lamps and the various test gases could be passed through zeolite traps cooled with liquid nitrogen or an alcohol/dry ice mixture. Cooled traps were absolutely necessary to remove trace impurities from these gases when used in the VUV lamp. Although high purity helium and argon were used (99.9999% helium or argon), no continuum was observed without prior removal of trace impurities.

Spectrometer Modifications

One objective of the current investigation involved the study of the transmission characteristics of helium over long path lengths and at high pressures up to approximately 20 atm. As implied by nomenclature, a VUV spectrometer is normally operated under vacuum conditions or at least under reduced pressures. Consequently, these instruments are designed to seal under reduced pressures but not if internal pressures exceed atmospheric pressure. Therefore, a number of modifications were required (1) to enable sealing of the sodium salicylate window under either vacuum or high pressure operating conditions, and (2) to prevent distortion of the thin metal plates forming the exit slit of the differential slit assembly. The detector flange supplied with the Model 630 detector assembly was replaced with an alternative flange system as shown in Fig. 19, which allowed changes in pressures from about 5×10^{-6} mm Hg to 20 atm without apparent leakage of gases or expulsion of the sodium salicylate holder against the photomultiplier tube. Similarly, two stainless steel inserts were machined and installed between the three 0.16 cm plates delineating the two differential slit assembly pumping chambers (see Fig. 20). These inserts contained ports at four positions to allow individual pumping of each chamber as originally designed and if required. The modified exit slit assembly was successfully operated at pressures approaching 20 atm without apparent distortion or damage.

Differential Slit Pressure and Flow Tests

A series of pressure and flow tests was conducted using the modified differential slit assembly to verify integrity of the optical slit system at pressures up to 20 atm. These tests also provide data with regard to pressure drops across the slit system and flow data for helium under high pressures. A schematic of the experimental layout used for these tests is shown in Fig. 21. A Fisher-Porter flow meter was used to monitor flow and was subsequently calibrated against a Matheson linear mass flow meter of known accuracy. Pressures in various chambers were monitored by means of pressure transducers in each chamber. Helium was used as the test gas during these studies and was exhausted to atmospheric pressure. Volumetric flow results obtained during these tests are shown in Fig. 22 as a function of upstream pressure (simulated test cell gas pressure). These results indicated that only the 10 μ slit would be usable for subsequent spectral studies in helium at pressures up to 20 atm. For example, a standard 1A cylinder of helium contains 6940 liters of gas at standard conditions. Extrapolating the volumetric flow data (Fig. 23) to 20 atm (for a 50 μ slit) indicates that a cylinder of helium would be expended in approximately fifteen minutes. Thus, subsequent spectroscopic data were obtained using only the 10 μ exit slit to permit long-duration tests.

Pressure data for various differential slit chambers, as well as simulated monochromator and test cell chambers, indicated that in each test all the pressure reduction occurred across the variable slit S_1. Negligible or no pressure drops occurred across slits S_2 and S_3 which were at fixed dimensions.

Experimental Procedures and Operating Parameters

All spectral measurements from approximately 60 to 300 nm were conducted in a windowless mode. No differential pumping was used for any of the tests conducted. A 2123 ℓ/minute auxiliary pump was used on the first chamber of the differential exit slit system to assist the spectrometer mechanical pump during actual measurements. With this arrangement, monochromator chamber pressure was always less than about 25 mm Hg. Helium and argon transmission measurements were made using the 61-cm-long test cell between the monochromator exit slit and the detector. A 1.91-cm-long cell was used for the UF_6 tests.

Standard quality helium and argon (99.995% rare gas) were used for the test gas except where noted. A pressure transducer of the appropriate range was used to monitor test gas pressures during various tests. Pressure transducer output was monitored on one channel of a two-channel recorder. The second recorder channel was used to monitor spectrometer detector output. Because of occasional rf interference from adjacent experiments in the laboratory, the pressure transducer output was also monitored on a Hewlett-Packard vacuum tube multirange volt meter. The rf interference caused erratic behavior of the recorder pressure transducer trace. A copper-

constantan thermocouple was used to monitor gas temperatures in the test cell. For helium and argon measurements, temperature was a constant 298 K for all tests. For the UF_6/argon tests, temperature was constant at 393 K, as monitored in the test cell and at various points in the gas handling-transfer system.

High-purity helium and argon (99.9999% rare gas) used as source-lamp gases required removal of trace impurities to allow significant intensity of their respective continua. The trap material was zerolite cooled with liquid nitrogen when helium was used and alchohol/dry ice mixture when argon was used. A trap was not required or used with xenon as the source gas. Gas pressures for the VUV sources were usually of the order of 50 to 120 mm Hg. No attempt was made to optimize the continuum emitted by the VUV lamp other than setting lamp pressure to maximize continuum output while minimizing the height of lines superimposed on the continuum.

In most cases, the spectrometer entrance slit was fixed at 50 μ and the exit slit at 10 μ. With these slit settings, the detector voltage and amplification and recorder gain were set to provide maximum recorder deflection with minimum noise.

Helium and argon spectra were scanned at 10 nm/minute while the rate of scanning for UF_6 spectra was 25 nm/minute. The higher scan rate for the UF_6 measurement was selected to minimize exposure of the equipment to UF_6 vapor.

Normal procedure included at least two I_o determinations in the evacuated system to insure stable operating conditions. Both lamp and monochromator pressure were monitored during these tests. For the rare gas transmission tests, the cell was filled to the required pressure and the flow allowed to equilibrate prior to conducting a wavelength scan. VUV lamp pressure, monochromator pressure, and cell pressure were recorded during the spectral scans. After a series of transmission measurements, usually one or two, the test cell was evacuated and either I_o redetermined or a selected wavelength (wavelength at the continuum peak) monitored to insure no changes had occurred during the preceding tests. I_o tests were made with both the diffusion pump and 425 ℓ/minute mechanical pump operating. Wavelength scans with the test gas were made with the 425 ℓ/minute and 2123 ℓ/minute mechanical pumps operating.

A similar procedure was followed for the UF_6 measurements. Initial I_o was determined in the evacuated system followed by an I_o' determination in which argon was allowed to flow in the test cell at a fixed pressure (no UF_6 flow). Subsequently, UF_6 was introduced into the cell, the pressure increase noted, and the wavelength scans with UF_6/argon were conducted. Upon completion of the spectral scan with UF_6/argon mixture, the UF_6 flow was terminated and the cell was pumped for approximately fifteen to twenty minutes to evacuate UF_6. As in previous tests with the rare gases, I_o' was redetermined or, for convenience, a particular peak in the previous I_o scan was monitored to insure constancy of conditions between scans. This procedure also served to establish that UF_6 contamination of the sodium salicylate had not occurred.

After two or three tests with UF_6, the sodium salicylate window was removed for visual inspection of UF_6 contamination. The sodium salicylate was routinely replaced at these times.

Spectral Results and Discussion of Results

Helium

A series of experiments was conducted in the apparatus, previously described, to determine the transmission properties of standard helium gas at high pressures. All transmission measurements were made in the 61-cm-long cell at room temperature. The wavelength ranges and helium pressures for which optical data were measured in this series of tests are summarized in TABLE VIII. TABLE VIII also includes pressure and wavelength ranges for two series of experiments involving helium from which contaminants were partially removed by a cooled zeolite trap and similar data for experiments with standard argon as the test gas.

Recorder traces of the relative spectral intensities determined during the experiments are shown in Figs. 23 through 26 for standard helium gas in the approximate wavelength range between 60 and 300 nm. Each figure illustrates I_o, the source intensity without test gas in the cell, and intensity scans I_1 and I_2 for two representative pressures of helium in the test cell. Additional experimental parameters (wavelength scan rates, slit settings, etc.) are listed in TABLE IX for each set of spectral measurements.

As the results illustrate, standard tank helium at pressures as low as 3.7 atm are relatively opaque in the VUV at wavelengths between 60 and 110 nm (see Fig. 23). At a pressure of 9 atm, the gas is almost totally opaque to VUV radiation. Figure 24 illustrates similar transmission data for standard tank helium between 100 and 160 nm. These results were obtained at 4.7 and 18.7 atm and show that the helium is relatively transparent in this wavelength interval. At a wavelength of about 128 nm, the transmission is approximately 65% at a helium pressure of 18.7 atm. Similar experimental results are shown in Fig. 25 in the wavelength range between 145 and 200 nm at helium pressures of 8.8 and 17.7 atm. The transmission of helium is of the order of 63% at a pressure of 17.7 atm and at a wavelength of 170 nm. Figure 26 illustrates the transmission properties of helium in the wavelength range between 220 and 300 nm for helium pressures of 5.4 and 18.3 atm. The results indicate that helium is relatively transparent in this wavelength range. For example, the transmission is of the order of 60% at a wavelength of 296 nm at a helium pressure of 18.3 atm.

As indicated by the spectral transmission results over a range of wavelengths and pressures, standard tank helium could be used as a transparent purge gas at high pressure approaching 20 atm in subsequent nuclear reactor tests at wavelengths greater than 100 nm. At wavelengths shorter than 100 nm, the standard tank gas is relatively opaque to radiation even at modest pressures (~ 4 atm).

Since the excited state population of room temperature helium is negligible, absorption of radiation in helium should occur only at wavelengths below 50 nm, the threshold for the boundfree continuum from the ground state. The marked attenuation of radiation in the wavelength interval between 60 and 100 nm is undoubtedly due to trace contaminants. These impurities are generally O_2, H_2, N_2, CO_2, and H_2O which constitute about 5×10^{-3} percent of the gas. Theoretical estimates of the the transmission of high purity helium (99.9999% helium), based on contaminant absorption coefficient data of reference 3, indicated about 30 percent transmission in high purity helium at 20 atm and over a path length of 60 cm in the VUV region.

Subsequently, a liquid-nitrogen-cooled zeolite trap was installed in the helium gas supply system to partially remove trace contaminants. A second series of transmission studies was conducted to determine the transmission properties of helium after removal of trace impurities. Spectral data (60 to 110 nm) at helium pressures of 7.3 and 18.5 atm are shown in Fig. 27. These data indicate that the transmission characteristics of helium are greatly improved if the helium is passed through a liquid-nitrogen-cooled, zeolite trap prior to the spectral measurements. Appreciable transmission was observed at helium pressures up to 18.5 atm with "clean" helium (Fig. 27) as compared to the untreated helium at 9 atm (Fig. 23).

Argon

Similar transmission measurements were made with standard tank argon (99.995%) in the spectral interval between 60 and 110 nm. These data were required to determine the approximate quantities of argon to be used in subsequent UF_6/argon tests and to provide basic transmission data related to the buffer gas region of a PCR. Typical experimental transmission results as a function of wavelength are shown in Fig. 28 for argon pressures of 0.13 and 0.46 atm. Argon is relatively opaque in this spectral region, as illustrated in Fig. 28. Since threshold for the first boundfree continuum in argon is at a wavelength of approximately 80 nm and extends to shorter wavelengths, no transmission was expected or observed below 80 nm. As in the case of helium, the marked attenuation of the radiation observed is probably due to trace contaminants. No attempts were made to remove contaminants as in the case of helium.

Uranium Hexafluoride

A series of transmission studies was conducted in mixtures of UF_6 and argon at various partial pressure ratios (P_{UF_6}/P_{Ar}). A summary of the pressures of argon and UF_6 as well as the corresponding partial pressure ratios used are tabulated in TABLE X. Other experimental parameters are shown in TABLE IX. All measurements were made at a temperature of 393 K and over a path length of 1.91 cm. The wavelength interval extended from 60 nm to approximately 200 nm.

Typical spectral transmission results for UF_6/argon mixtures are shown in Fig. 29 for the wavelength interval between 60 and 120 nm and in Fig. 30 for the wavelength interval between 120 and 200 nm. Curve 1 represents the relative source intensity I_o, without gases in the test cell, while curve 2 shows the relative intensity I_o', after introduction of argon into the cell at a pressure of 45.8 mm Hg. Curves 3 and 4 illustrate the transmission spectra of UF_6/argon mixtures with UF_6 partial pressures of 1.78 and 0.48 mm Hg, respectively. Similar data were obtained for the other conditions listed in TABLE X. A partial pressure of less than 2 mm Hg of UF_6 reduces the transmission by about 85 percent throughout this spectral region.

The results displayed in Fig. 29 were used to determine absorption cross sections for UF_6 in the VUV region. The cross section is defined by the relationship:

$$I/I_o' = \exp - \sigma NL \qquad (3)$$

where I is the transmitted intensity, I_o' is the incident intensity; σ the absorption cross section, N the absorber density, and L the path length (1.91 cm). The incident intensity used in these calculations was I_o', the relative intensity with argon in the test cell (Fig. 29, curve 2). The quantity I/I_o' was determined at wavelength intervals of 2.5 nm between 80 and 120 nm. These data (I/I_o') are plotted as a function of wavelength in Figs. 31 and 32 for five partial pressures of UF_6 investigated. Number densities were determined from knowledge of the UF_6 pressure (TABLE X) and temperature as follows:

$$N = 7.341 \times 10^{21} \frac{P(atm)}{T} \qquad (4)$$

Subsequently, cross section data were calculated for the five sets of experimental data by means of Eq. (3);

$$\sigma = -(\ln \frac{I}{I_o'})/NL \qquad (5)$$

These results are summarized in TABLE XI. The last colum in TABLE XI are the calculated average values of the absorption cross section at various wavelengths. Average cross section results are graphically illustrated in Fig. 33 as a function of wavelength.

The cross section results shown in TABLE XI and Fig. 33 exhibit a range of values from about 6×10^{-18} to 2.7×10^{-17} cm^2. As shown in Fig. 33, the data below approximately 95 nm, are reasonably smooth with relatively small scatter. At wavelengths greater than 95 nm, determination of the relative intensities with accuracy is difficult due to the low intensity from the VUV source. Thus, small errors in determining I_o or I or random noise on the traces result in the scatter observed in the data at wavelengths greater than 95 nm.

TABLE I

SUMMARY OF EXPERIMENTAL CONDITIONS FOR EMISSION STUDIES

(Lithium Fluoride Window, $120 < \lambda < 580$ nm)

$P_{total} = 1.0$ atm

No.	Temp. deg K	$\dot{m}_{UF_6}$ g/s	$\dot{m}_{Ar}$ g/s	P_{UF_6} mm	$\dot{m}_{UF_6}/\dot{m}_{Ar}$
1	810	0.062	0.79	6.8	7.9×10^{-2}
2	1070	0.056	1.46	3.2	3.8×10^{-2}
3	1030	0.016	1.21	1.1	1.3×10^{-2}
4	1260	0.010	1.08	0.80	9.3×10^{-3}
5	1320	0.046	2.49	1.6	1.8×10^{-2}
6	1330	0.048	1.93	2.2	2.6×10^{-2}
7	1330	0.035	2.49	1.2	1.4×10^{-2}
8	1330	0.050	2.49	1.7	2.0×10^{-2}
9	1340	0.012	1.46	0.71	8.2×10^{-3}
10	1360	0.002	1.08	0.16	1.9×10^{-3}
11	1400	0.065	2.49	2.3	2.6×10^{-3}
12	1400	0.065	3.16	1.8	2.1×10^{-2}
13	1400	0.042	1.47	2.5	2.9×10^{-2}
14	1510	0.014	2.49	0.48	5.6×10^{-3}
15	1510	0.011	1.10	0.86	1.0×10^{-2}
16	1530	0.020	2.49	0.70	8.0×10^{-3}
17	1680	0.12	1.48	6.9	8.1×10^{-2}
18	1730	0.11	3.49	2.7	3.2×10^{-2}
19	1810	0.012	1.46	0.71	8.2×10^{-3}
20	1860	0.043	3.49	1.1	1.2×10^{-2}
21	2060	0.0086	4.71	0.16	1.8×10^{-3}
22	2300	0.0084	5.08	0.14	1.7×10^{-3}
23	2430	0.0056	5.08	0.10	1.1×10^{-3}
24	2740	0.016	5.46	0.25	2.9×10^{-3}
25	2770	0.026	4.91	0.53	5.3×10^{-3}
26	3560*	0.013	5.46	0.21	2.4×10^{-3}

*Estimated value, see text for discussion.

TABLE II

SUMMARY OF TOTAL INTENSITIES
INTEGRATED BETWEEN 300 AND 500 NM

Temperature K	Run No.*	Intensity $I_t(T)$
810	1	1.63×10^{-4}
1050	2,3	4.12×10^{-1}
1260	4	1.38×10^{1}
1340	5 thru 10	1.55×10^{3}
1400	11, 12, 13	3.78×10^{3}
1520	14, 15, 16	6.45×10^{3}
1710	17, 18	2.78×10^{4}
1840	19, 20	4.43×10^{4}
2060	23	7.46×10^{4}
2300	22	1.11×10^{5}
2430	23	1.62×10^{5}
2760	24, 25	2.43×10^{5}
3650	26	7.21×10^{5}

*Denotes runs which were averaged.

TABLE III

SUMMARY OF FRACTIONAL INTENSITIES AT VARIOUS TEMPERATURES

Wavelength Interval nm	Fractional Intensities												
	3560°K	2740°K	2430°K	2300°K	2060°K	1810°K	1700°K	1500°K	1400°K	1330°K	1260°K	1050°K	810°K
300-340	4.72	3.51	4.76	3.68	3.47	2.12	1.53	1.67	1.17	0.44	0.49	0.094	0.012
340-380	8.64	7.15	8.52	7.28	8.56	6.83	5.12	4.56	4.00	2.09	1.73	0.790	0.223
380-420	15.50	15.70	14.30	15.20	14.80	11.90	9.19	12.90	9.26	8.27	10.41	6.880	7.460
420-460	20.30	21.80	21.50	22.20	22.90	20.40	20.50	22.70	21.00	23.20	22.40	23.400	32.100
460-500	19.30	19.90	20.10	20.50	19.20	22.30	23.10	22.20	24.40	24.40	23.50	25.500	31.300
500-540	17.10	17.90	17.20	17.70	17.00	20.20	21.70	19.90	21.40	22.80	22.10	23.000	22.800
540-580	14.50	14.80	13.60	13.40	14.20	16.90	18.80	16.20	18.20	19.70	19.50	20.300	7.090

TABLE IV

SUMMARY OF EXPERIMENTAL CONDITIONS FOR EMISSION STUDIES

(Windowless Mode, $80 < \lambda < 300$ nm)

$P_{total} = 1.0$ atm

No.	Temp. K	$\dot{m}_{UF_6}$ g/s	$\dot{m}_{Ar}$ g/s	P_{UF_6} mm Hg	$\dot{m}_{UF_6}/\dot{m}_{Ar}$
27	1050	.043	1.46	2.53	2.5×10^{-2}
28	1400	.044	2.49	1.52	1.8×10^{-2}
29	2280	.046	5.10	0.78	9.02×10^{-3}

TABLE V

SUMMARY OF EXPERIMENTAL
CONDITIONS FOR EMISSION STUDIES AT HIGH PRESSURES

(Lithium Fluoride Window, $120 < \lambda < 600$ nm)

No.	Temp K	$\dot{m}_{UF_6}$ g/s	$\dot{m}_{Ar}$ g/s	P_{UF_6} mm Hg	$\dot{m}_{UF_6}/\dot{m}_{Ar}$	P_{total} atm
30	1050	.056	1.46	3.29	3.8×10^{-2}	1.22
31	1350	.044	1.93	1.96	2.3×10^{-2}	1.37
32	1880	.012	3.49	2.96	3.4×10^{-3}	1.63
33	2030	.043	4.71	0.79	9.1×10^{-3}	1.62
34	2410	.009	5.08	0.15	1.8×10^{-3}	1.73

TABLE VI

SUMMARY OF EXPERIMENTAL CONDITIONS FOR ABSORPTION STUDIES

(Lithium Fluoride Window, 420 nm < λ <580 nm)

P_{total} = 1.0 atm

No.	Temp. K	$\dot{m}_{UF_6}$ g/s	$\dot{m}_{Ar}$ g/s	P_{UF_6} mm Hg	$\dot{m}_{UF_6}/\dot{m}_{Ar}$
A	980	0.091	0.79	9.8	.12
B	1050	0.095	0.79	10.0	.12
C	1270	0.107	1.46	6.3	.073
D	1440	0.102	1.46	6.0	.070
E	1770	0.099	1.46	5.8	.068

TABLE VII

SUMMARY OF "EFFECTIVE" CROSS SECTIONS
AT VARIOUS TEMPERATURES

Wavelength nm	← Cross-Section, cm^2 →				
	T = 980 K	1050 K	1270 K	1440 K	1770 K
420	5.75-19	6.03-19	8.54-19	6.02-19	4.82-19
430	5.21	5.46	7.52	4.99	4.53
440	4.71	4.94	6.64	4.06	4.21
450	4.24	4.45	5.82	3.31	3.92
460	3.85	4.03	5.09	2.63	3.64
470	3.51	3.68	4.43	2.17	3.29
480	3.18	3.33	3.84	1.84	3.05
490	2.91	3.05	3.34	1.57	2.74
500	2.71	2.84	2.92	1.36	2.50
510	2.55	2.67	2.59	1.18	2.30
520	2.44	2.56	2.38	1.10	2.10
530	2.40	2.52	2.26	1.02	1.97
540	2.44	2.56	2.28	9.69-20	1.83
550	2.53	2.66	2.40	8.91	1.90
560	2.71	2.84	2.66	8.91	1.93
570	2.98	3.13	3.07	8.91	2.10
580	3.38	3.54	3.69	8.91	2.30

TABLE VIII

PRESSURES AND WAVELENGTH RANGES FOR RARE GAS MEASUREMENTS

Gas	Wavelength Range (nm)	Pressure (atm)	Gas	Wavelength Range (nm)	Pressure (atm)
Helium (99.995%)	60-110	0.20	Helium (99.995%)	220-300	1.21
		0.45			5.39
		0.79			8.87
		1.13			13.59
		1.49			18.30
		3.66			
		4.75	Helium*		
		7.46	(99.995%)	60-110	1.31
		9.01			3.45
					4.51
Helium					7.32
(99.995%)	105-150	0.93			14.08
		3.31			18.52
		4.72			
		6.34	Argon		
		10.70	(99.995%)	60-110	0.11
		12.81			0.29
		18.66			0.45
					0.46
Helium					
(99.995%)	145-200	1.35			
		5.17			
		8.80			
		13.70			
		17.74			

* Liquid nitrogen cooled zeolite trap used for helium test gas - all others, no trap

TABLE IX

SUMMARY OF EXPERIMENTAL PARAMETERS

Test Gas and Wavelength Range (nm)	UV Source	Detector	Wavelength Scan Rate nm/min	Slit Width Entrance-exit μm	Path Length cm
Helium-99.995% 60-110	Helium Continuum P_{He} = 122 mm Hg Air-gap Spark-20 ma	1175 V 0.3 μA scale	10	50-10	61
Helium-99.995% 100-160	Argon Continuum P_{Ar} = 110 mm Hg Air-gap Spark-20 ma	1150 V 0.3 μA scale	10	50-10	61
Helium-99.995% 145-200	Xenon Continuum P_{Xe} = 110 mm Hg Air-gap Spark-20 ma	1175 V 0.3 μA scale	10	50-10	61
Helium 99.995% 220-300	Quartz-iodine, tungsten filament lamp - 8.3 amp	1175 V 0.3 μA scale	10	50-10	61
Helium-99.995% 60-110 (with cooled zeolite trap)	Helium Continuum P_{He} = 121 mm Hg Air-gap Spark-20 ma	1125 V 0.1 μA scale	10	50-10	61
Argon-99.995% 60-110	Helium Continuum P_{He} = 110 mm Hg Air-gap Spark-20 ma	1200 V 0.3 μA scale	10	50-10	61
UF_6/Argon 60-200	Helium Continuum P_{He} = 95 mm Hg Air-gap Spark-20 ma	1200 V 0.3 μA scale	25	50-10	1.91

TABLE X

UF_6 AND ARGON PRESSURES AND UF_6/Ar PRESSURE RATIOS USED FOR SPECTRAL ABSORPTION MEASUREMENTS

Series	P_A, mm Hg	P_{UF_6}, mm Hg	P_{UF_6}/P_{Ar}
A-1	31.5	0.62	1.97×10^{-2}
A-2	31.5	0.22	6.98×10^{-3}
A-3	31.5	1.72	5.46×10^{-2}
B-1	45.8	1.71	3.73×10^{-2}
B-2	45.8	0.48	1.05×10^{-2}

TABLE XI

ABSORPTION CROSS SECTIONS OF URANIUM HEXAFLUORIDE

Superscripts A and B and Subscripts 1, 2, and 3
Refer to Test Series Pressures Given in TABLE X

λ nm	σ_1^A	σ_2^A	$\sigma_{3_2}^A$	σ_1^B	σ_2^B	(σ)
	← cm^2 →					
80.0	1.37-17	--	--	1.84-17	1.09-17	1.43-17
82.5	1.31-17	5.80-18	2.18-17	1.75-17	1.31-17	1.42-17
85.0	1.68-17	9.58-18	2.22-17	2.24-17	1.42-17	1.70-17
87.5	1.46-17	1.19-17	2.29-17	2.41-17	1.56-17	1.78-17
90.0	1.76-17	1.40-17	2.67-17	2.56-17	1.64-17	2.01-17
92.5	1.91-17	1.54-17	2.53-17	2.95-17	1.77-17	2.14-17
95.0	1.94-17	2.06-17	--	3.66-17	2.53-17	2.55-17
97.5	2.18-17	1.70-17	--	2.84-17	2.45-17	2.29-17
100.0	2.20-17	2.50-17	--	2.82-17	3.19-17	2.68-17
102.5	--	--	--	1.45-17	1.63-17	1.54-17
105.0	2.32-17	--	--	1.79-17	1.32-17	1.81-17
115.0	--	--	--	1.93-17	1.45-17	1.69-17
117.5	--	--	--	6.98-18	5.74-18	6.36-17
120.0	--	--	--	6.51-18	1.28-17	8.66-18

(-) Denotes an average value

FIG. 1

SCHEMATIC OF A UNIT CAVITY OF A PLASMA CORE REACTOR

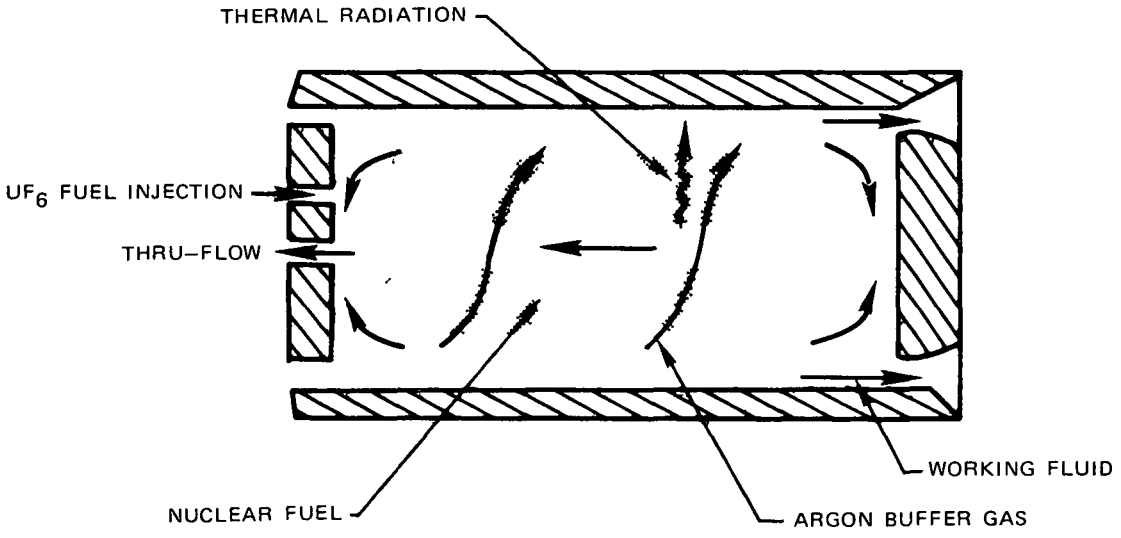

FIG. 2

SCHEMATIC OF UF_6 PLASMA TORCH SYSTEM

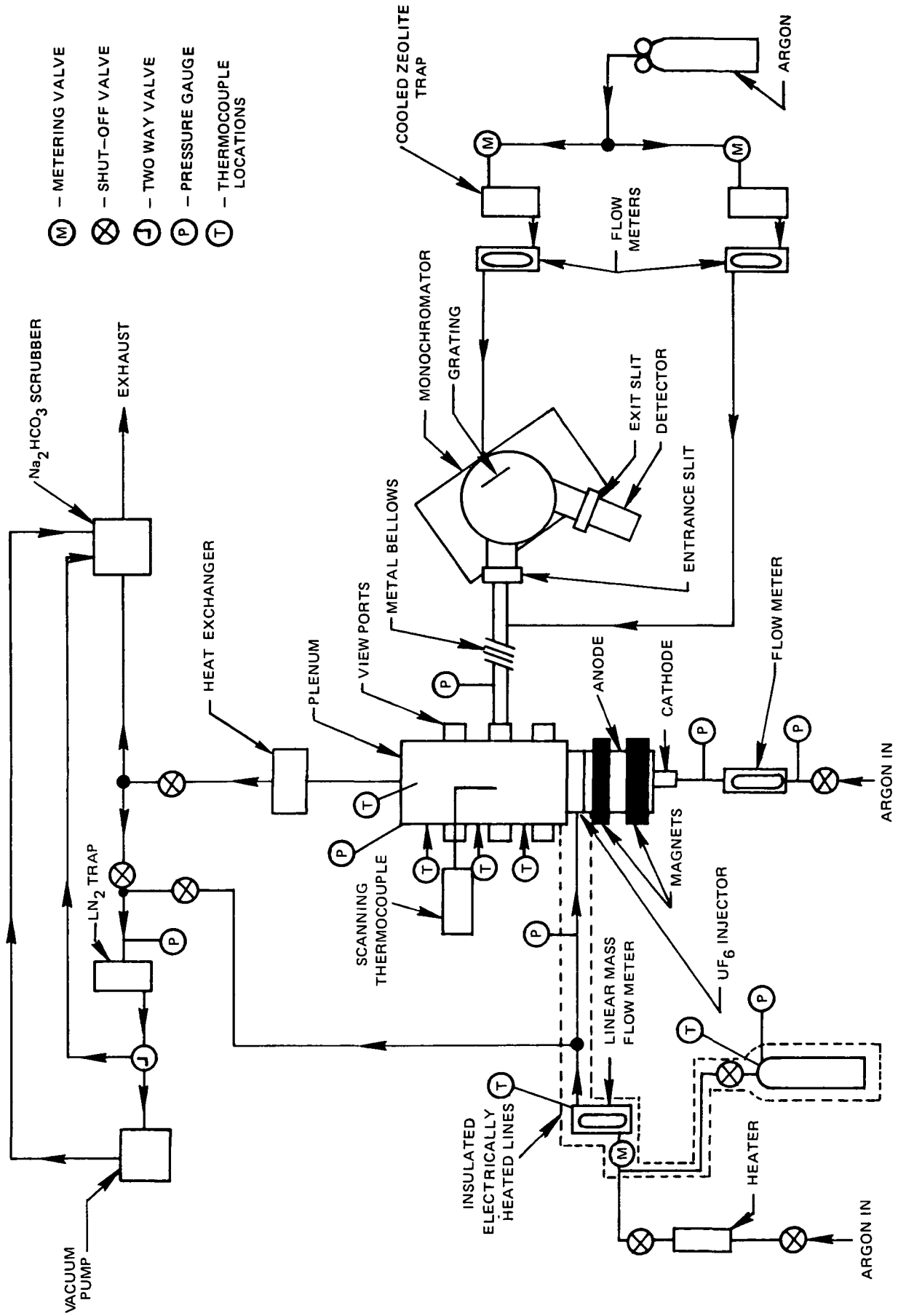

FIG. 3

UF_6 PLASMA TORCH

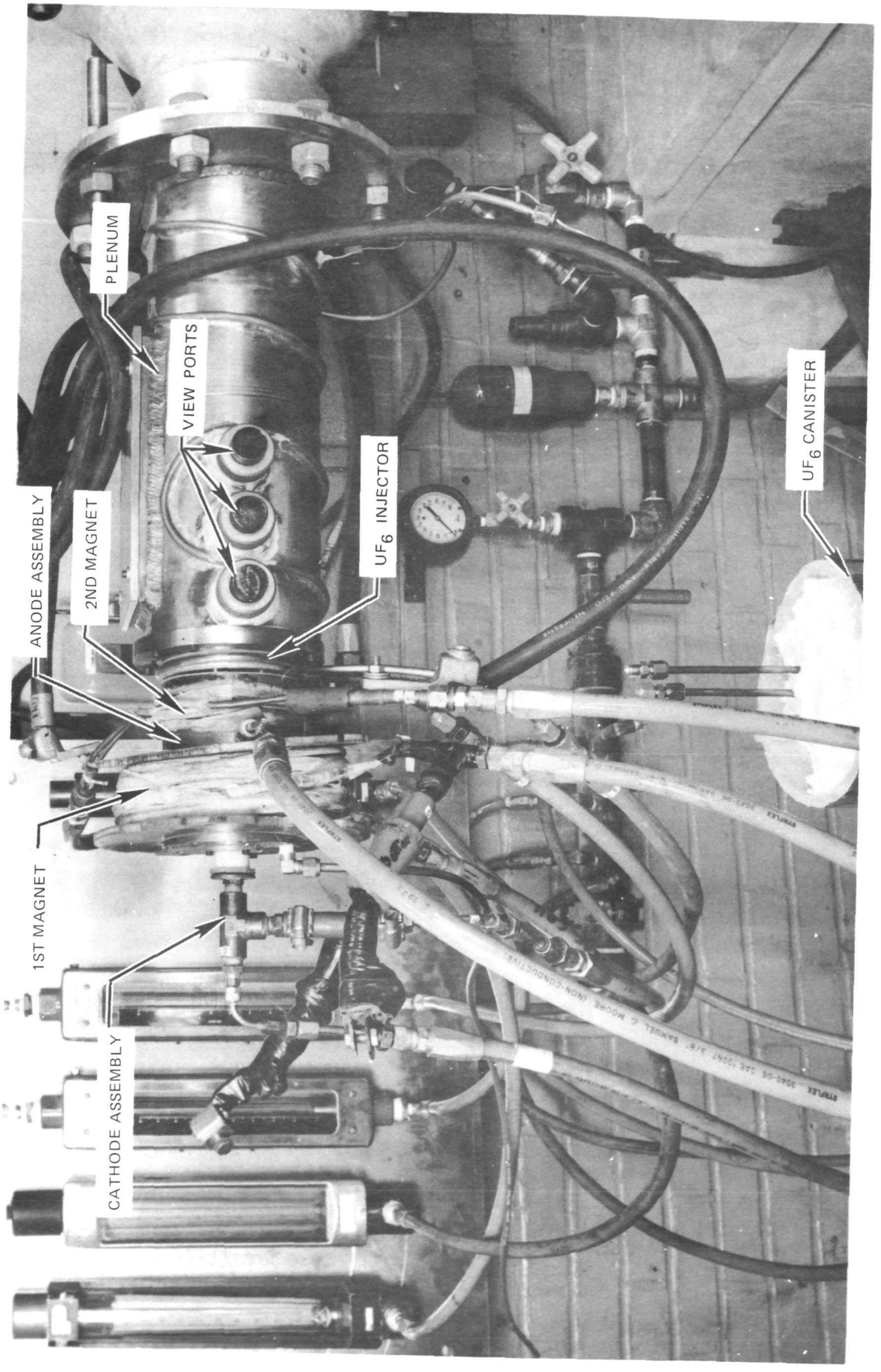

76–04–68–1

FIG. 4

SCHEMATIC OF PLASMA TORCH ASSEMBLY

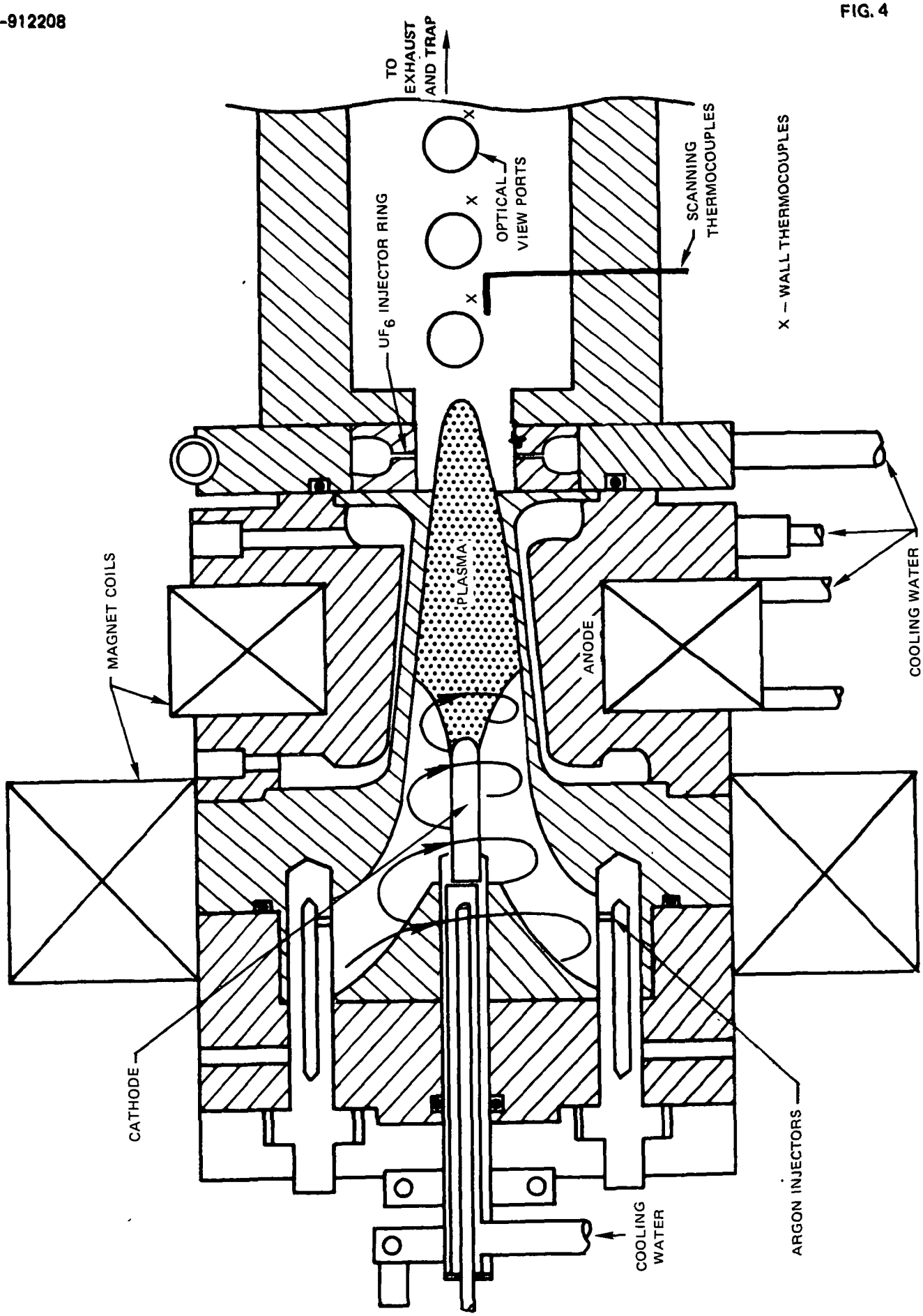

FIG. 5

TYPICAL TEMPERATURE PROFILES ALONG THE OPTICAL PATH IN THE PLENUM

(DATA TAKEN AT OPTICAL PORT ADJACENT TO UF_6 INJECTOR)

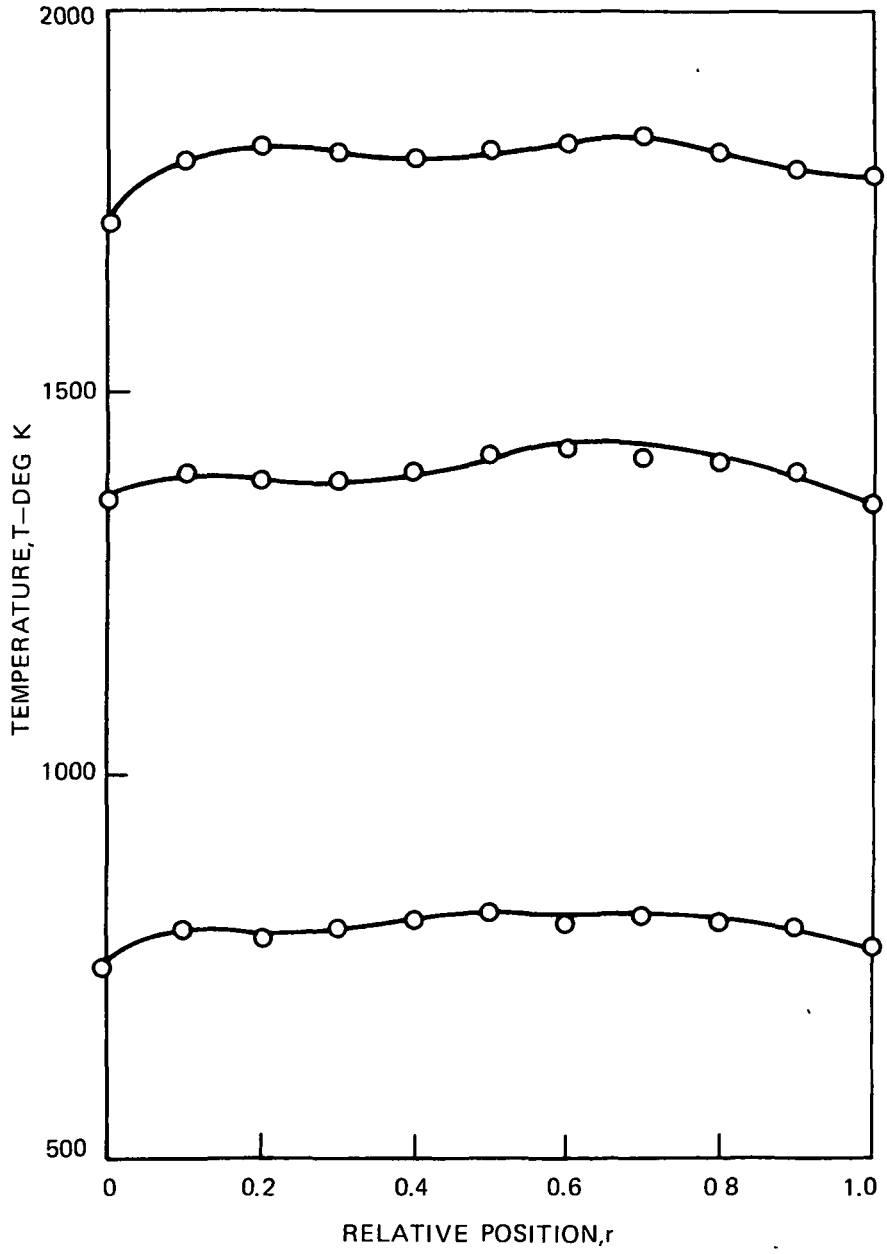

COMPARISON OF THE RELATIVE SPECTRAL INTENSITY OF URANIUM HEXAFLUORIDE AT VARIOUS TEMPERATURES BETWEEN 1000 AND 3600 DEG K

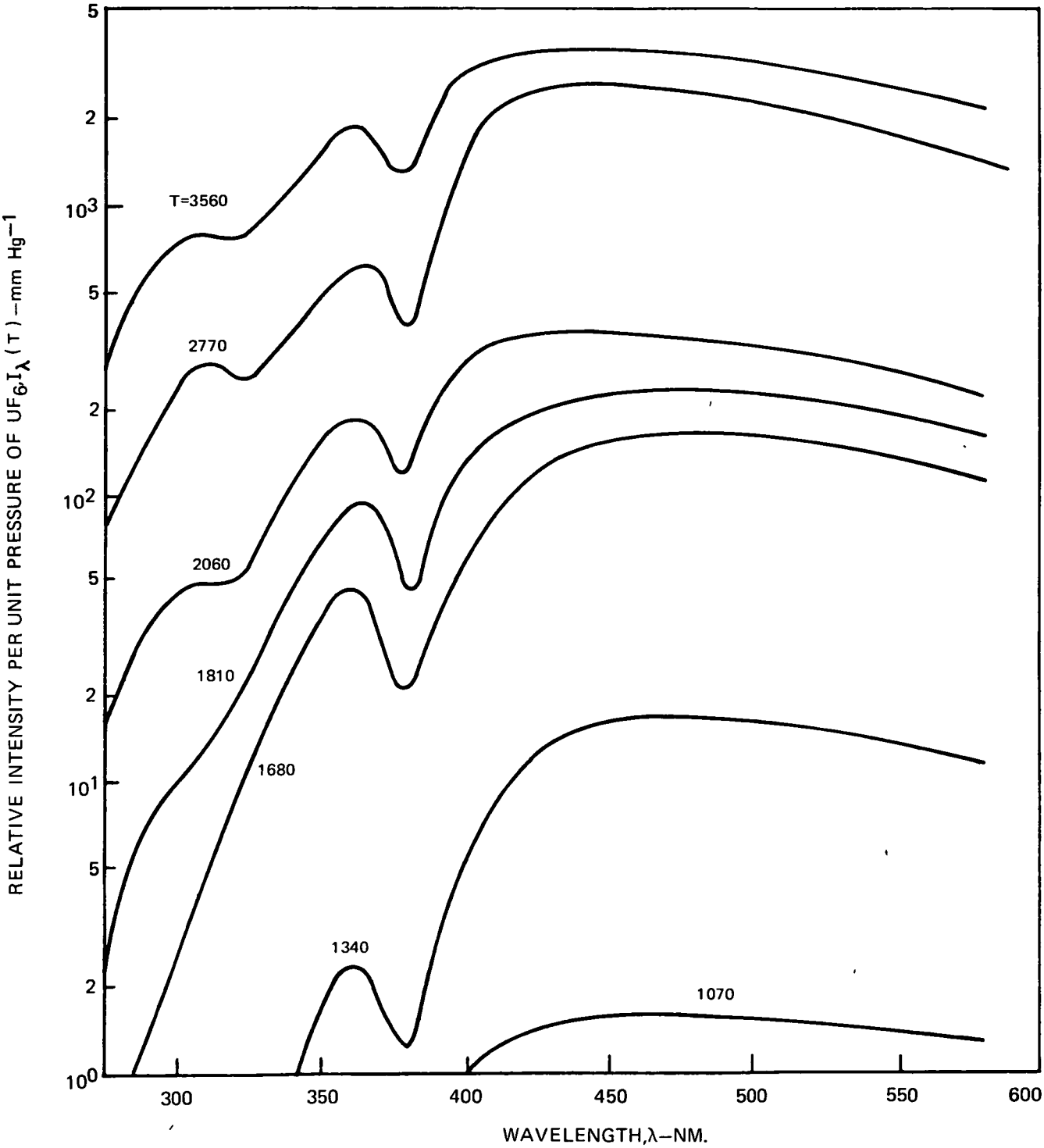

FIG. 7

NORMALIZED INTEGRATED INTENSITY FROM 300 TO 580 NM AS A FUNCTION OF TEMPERATURE

$$I_t(T) = \int_{300}^{580} I_\lambda(T)\, d\lambda \Big/ \int_{300}^{580} I_\lambda(3560) d\lambda$$

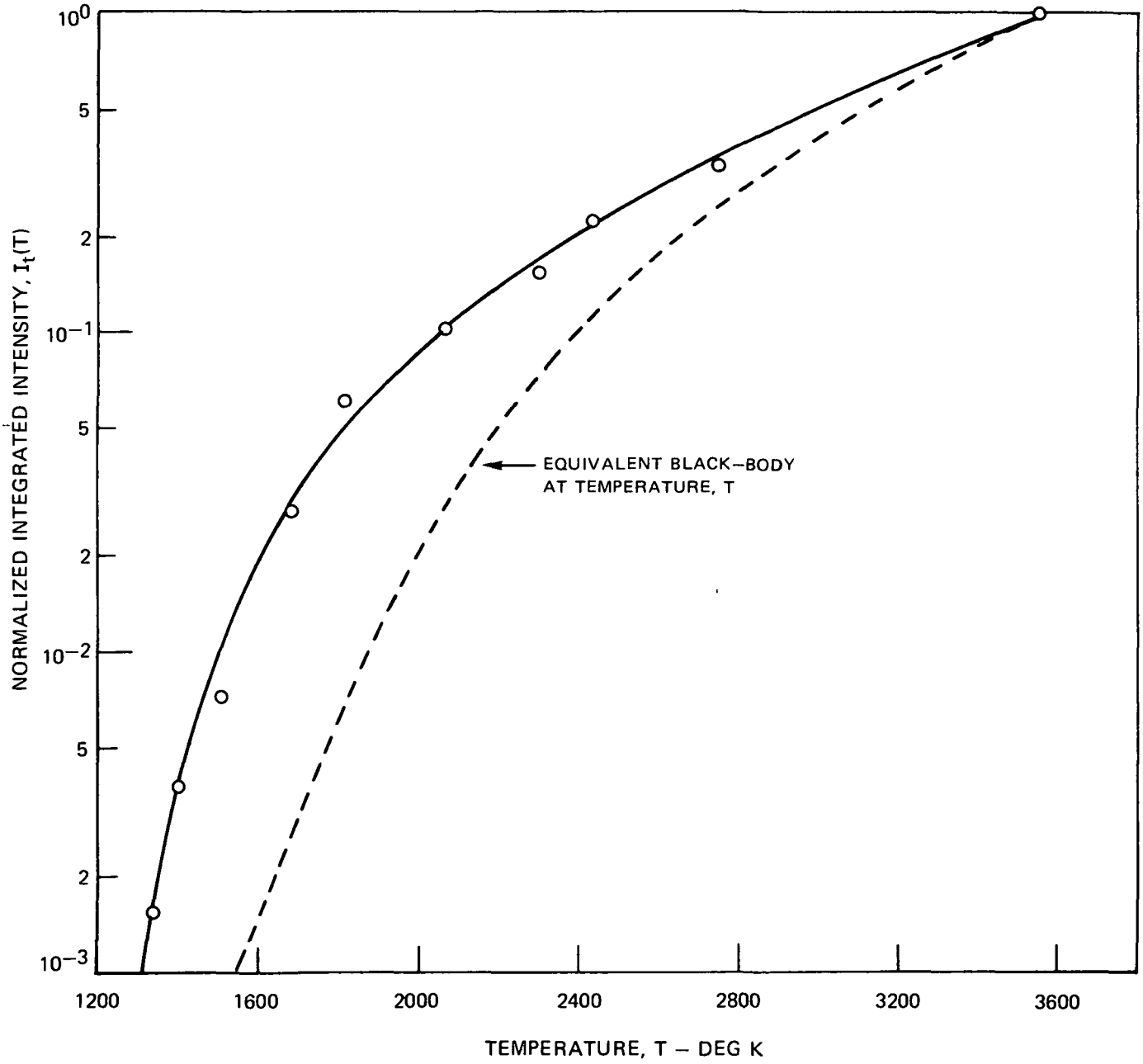

76–05–13–2

FRACTIONAL INTEGRATED INTENSITY PER 40 NM WAVELENGTH INTERVALS

$$I_{\Delta\lambda}(T) = \frac{\int_{\Delta\lambda = 40} I_\lambda\,(T)\,d\lambda}{\int_{300}^{580} I_\lambda\,(T)\,d\lambda}$$

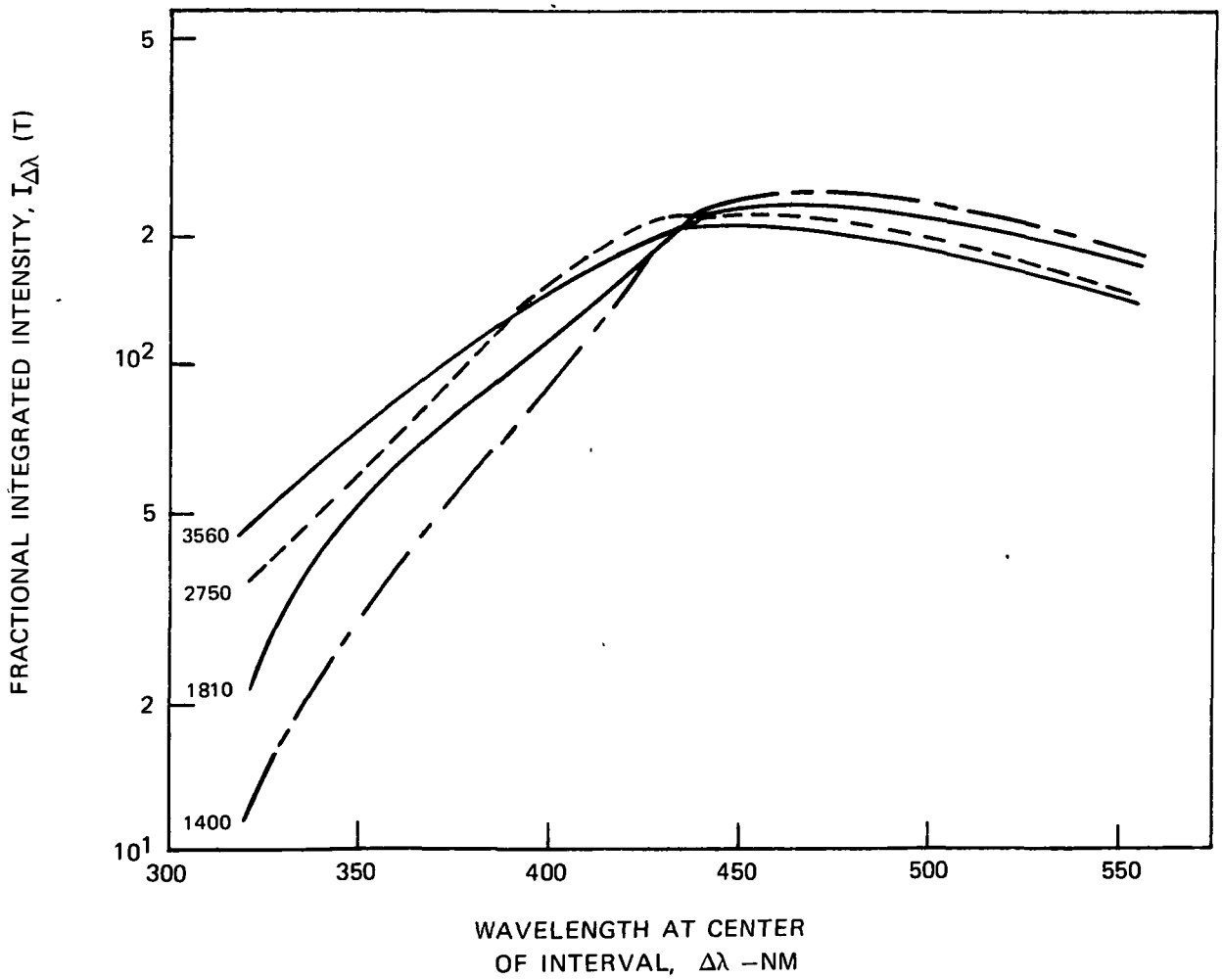

FIG. 9

COMPOSITION OF UF_6/ARGON MIXTURE AS A FUNCTION OF TEMPERATURE

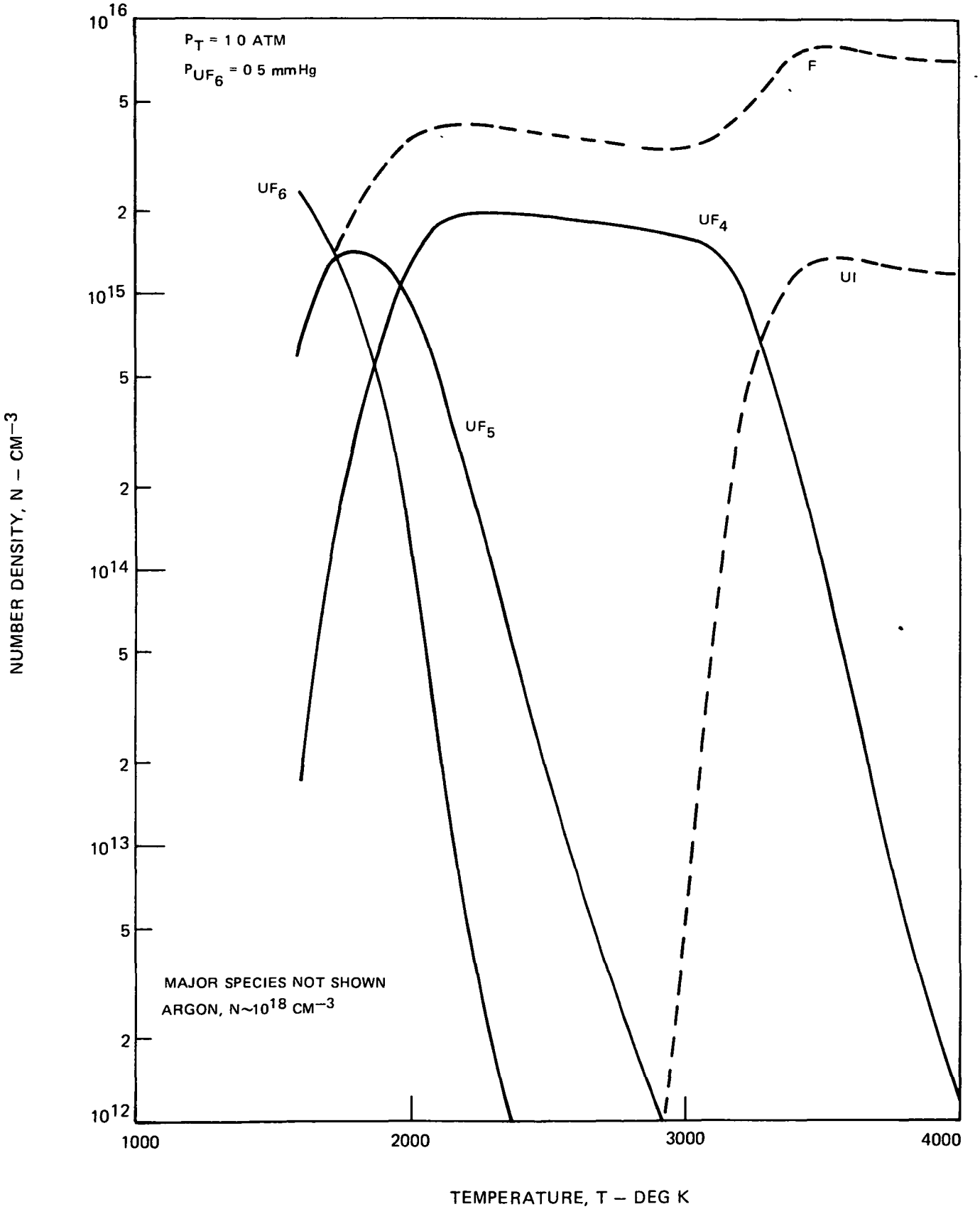

76–05–13–1

COMPOSITION OF UF_6/ARGON MIXTURE AS A FUNCTION OF TEMPERATURE

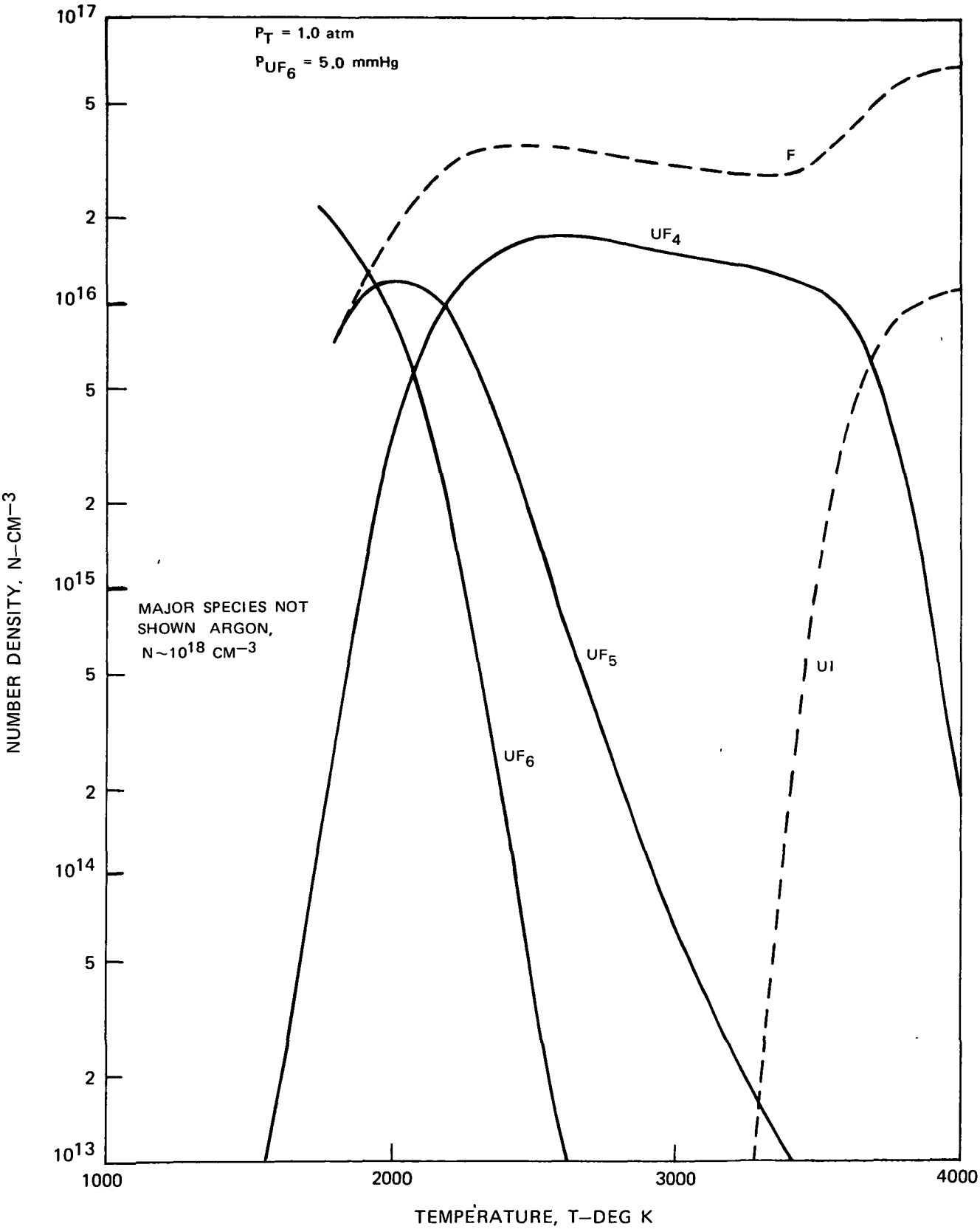

76–05–15–1

FIG. 11

COMPARISON OF RELATIVE SPECTRAL EMISSION AT TOTAL PRESSURES OF 1.0 AND 1.73 ATM

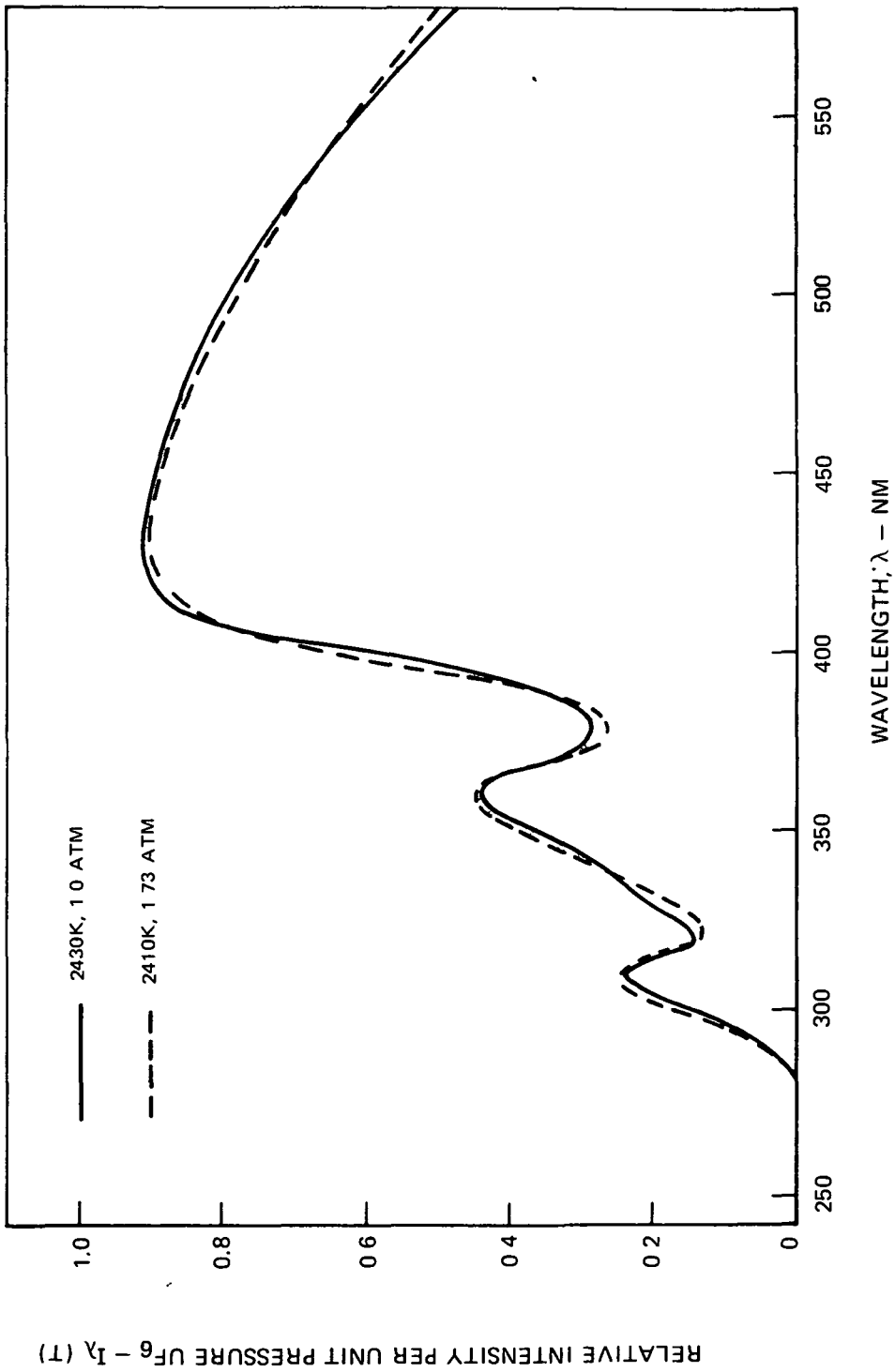

FIG. 12

TYPICAL RELATIVE INTENSITY RESULTS FOR ABSORPTION MEASUREMENTS

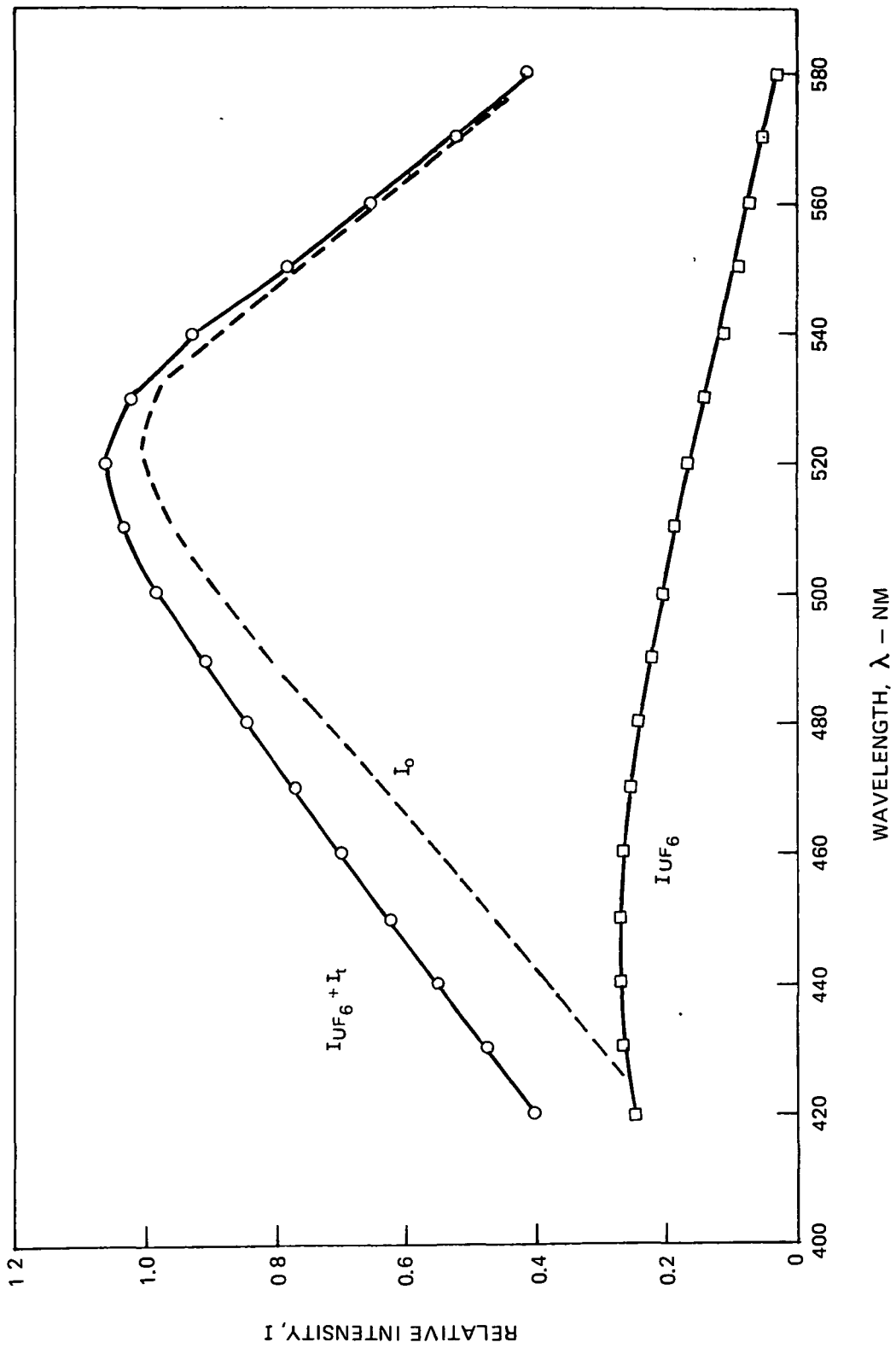

RELATIVE SPECTRAL TRANSMISSION AT VARIOUS TEMPERATURES

SYM.	NO.	T	MASS FLOW g/SEC		P_{UF_6}
		K	UF_6	Ar	mmHg
●	A	980	.091	0.79	9.8
◇	B	1050	095	0.79	10 0
○	C	1270	.107	1.46	6.3
□	D	1440	102	1.46	6.0
△	E	1770	.099	1.46	5.8

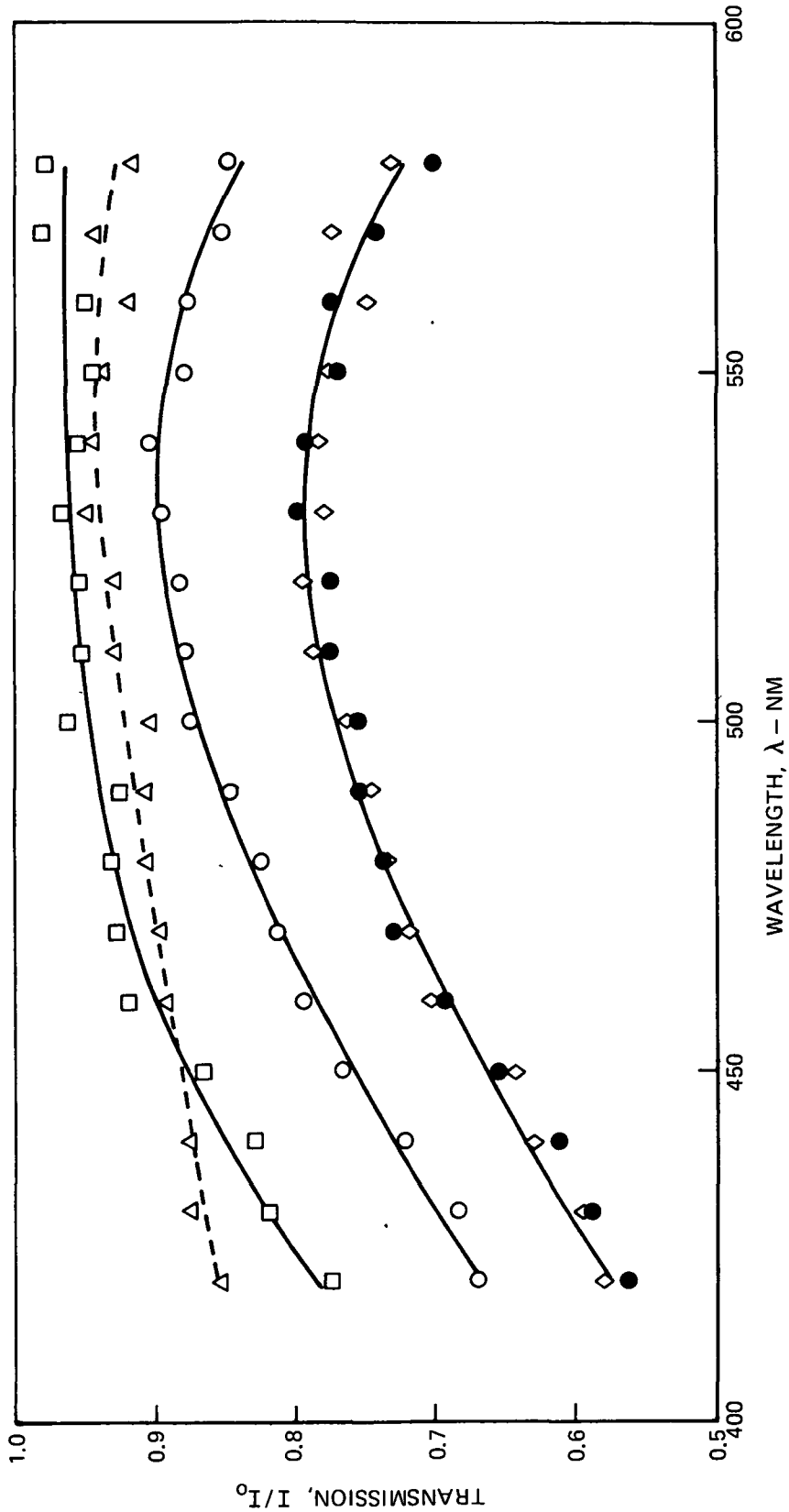

FIG. 14

"EFFECTIVE" SPECTRAL CROSS–SECTION AT VARIOUS TEMPERATURES

NO.	T	MASS FLOW g/SEC		P_{UF_6}
	K	UF_6	Ar	mm Hg
A	980	0.091	0 79	9 8
B	1050	0 095	0 79	10 0
C	1270	0 107	1.46	6 3
D	1440	0 102	1 46	6.0
E	1770	0 099	1 46	5 8

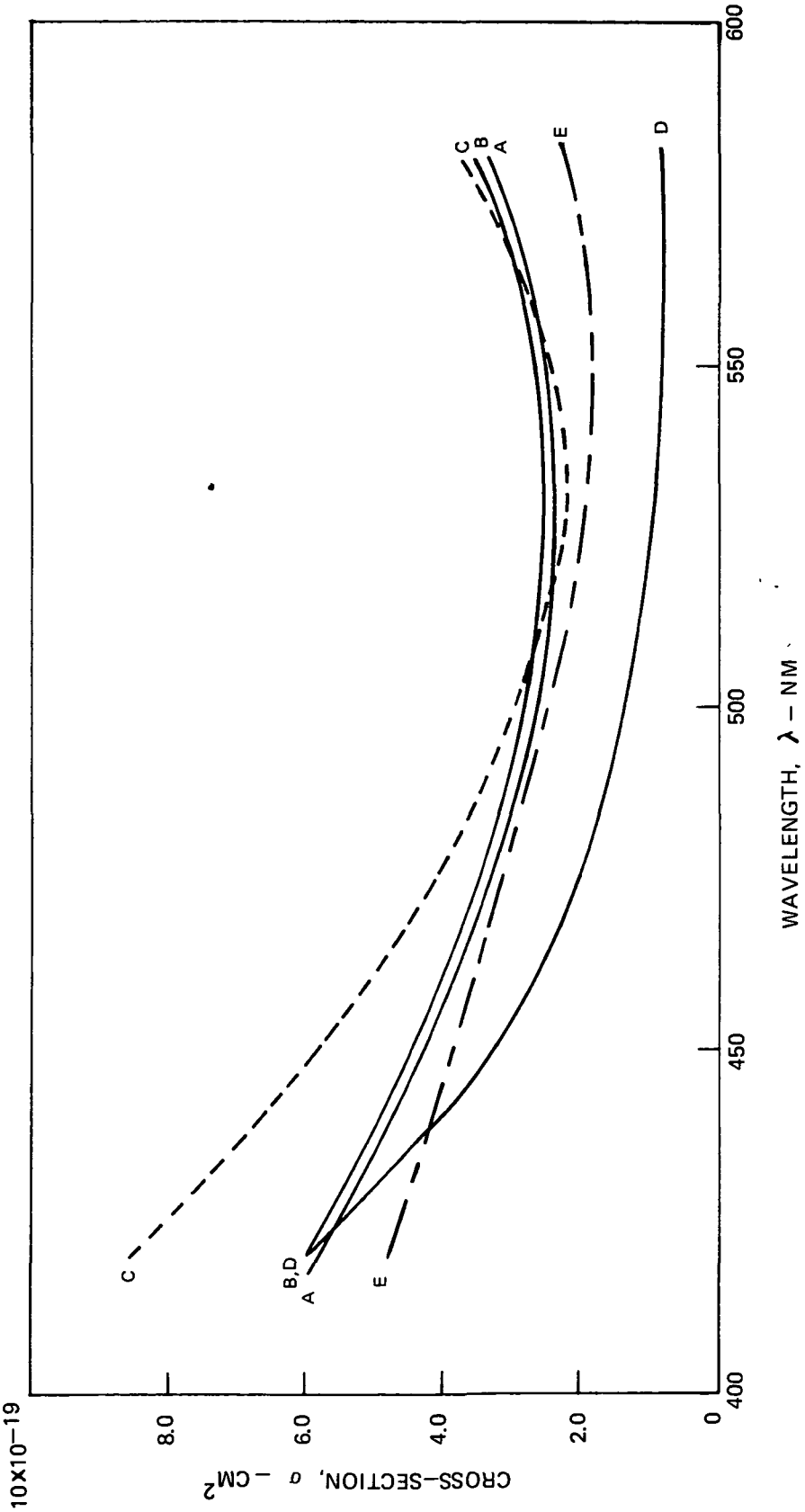

FIG. 15

TYPICAL IR SPECTROPHOTOMETRIC TRACE OF A DEPOSIT SAMPLE

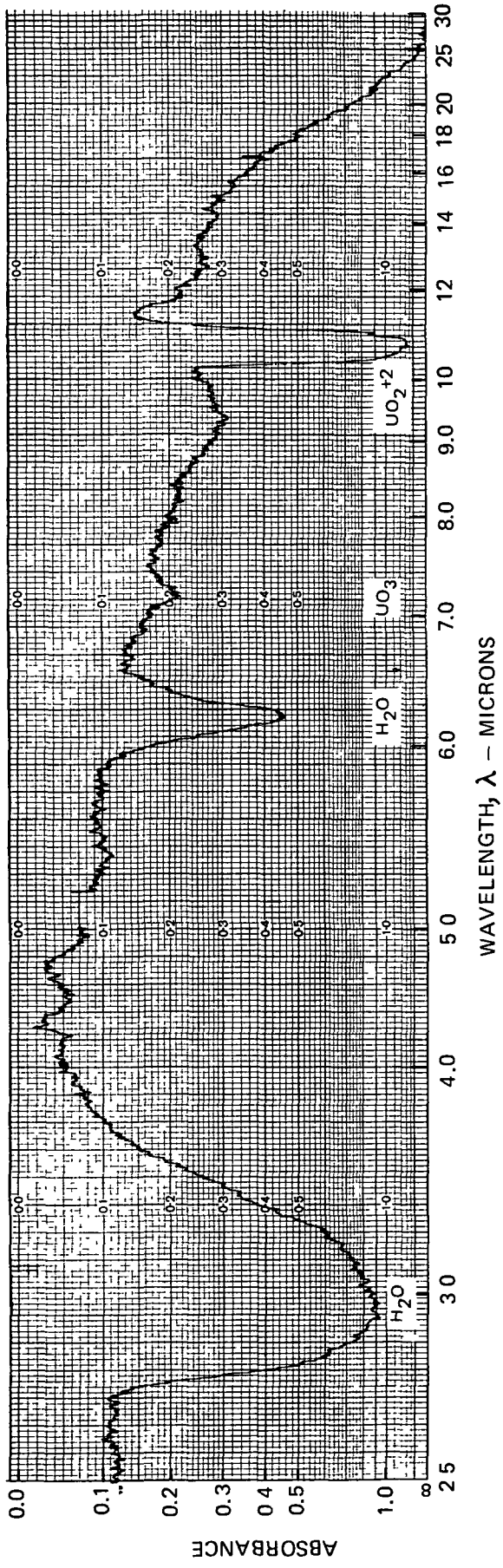

FIG. 16

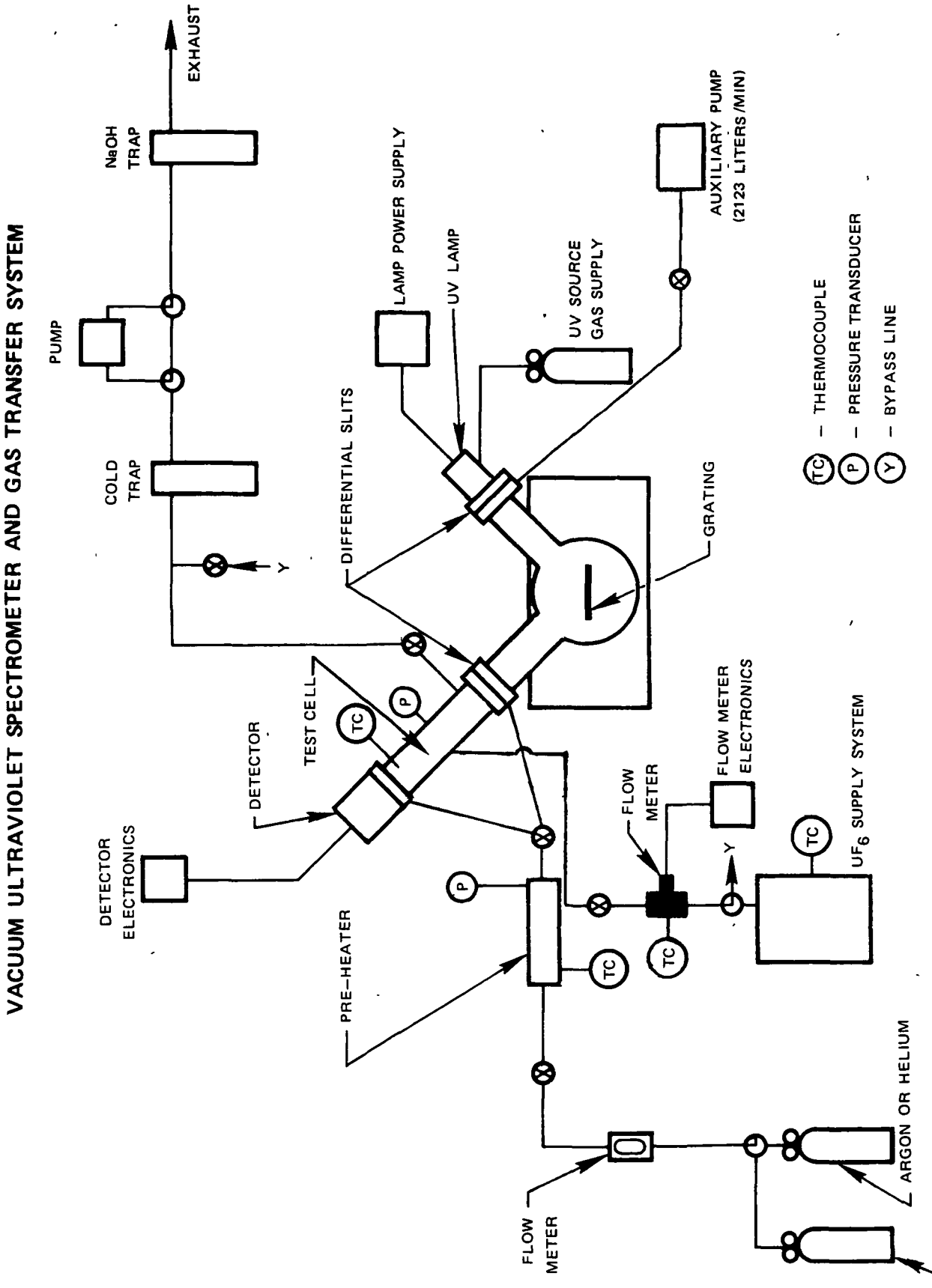
VACUUM ULTRAVIOLET SPECTROMETER AND GAS TRANSFER SYSTEM
EXHAUST
NaOH TRAP
PUMP
COLD TRAP
Y
DIFFERENTIAL SLITS
LAMP POWER SUPPLY
UV LAMP
UV SOURCE GAS SUPPLY
AUXILIARY PUMP (2123 LITERS/MIN)
GRATING
TEST CELL
DETECTOR
DETECTOR ELECTRONICS
PRE-HEATER
FLOW METER
FLOW METER ELECTRONICS
UF6 SUPPLY SYSTEM
FLOW METER
ARGON OR HELIUM
N2 PURGE GAS
TC – THERMOCOUPLE
P – PRESSURE TRANSDUCER
Y – BYPASS LINE

VACUUM ULTRAVIOLET SPECTROMETER SYSTEM

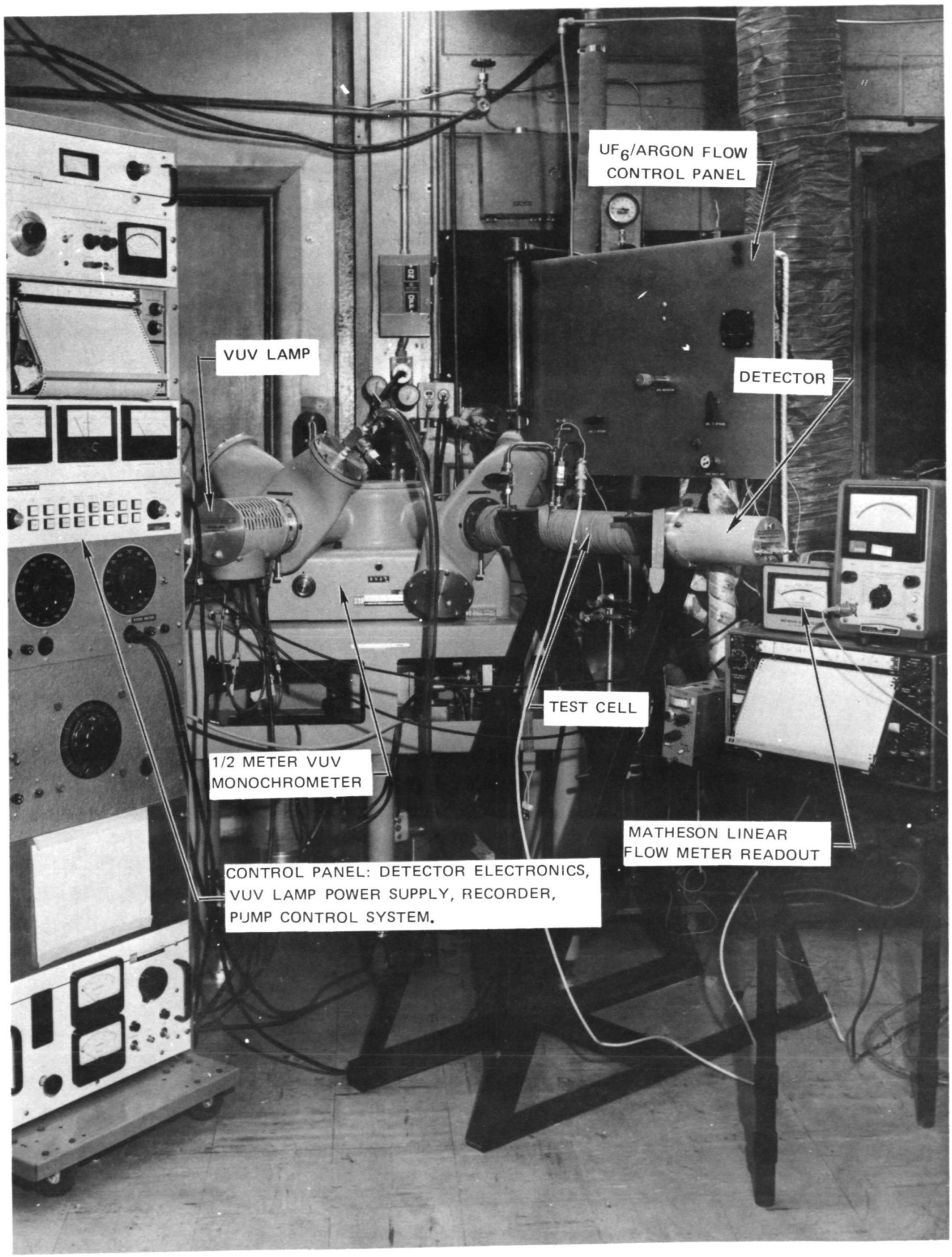

FIG. 18

SCHEMATIC OF UF_6/ARGON TEST CELL CONFIGURATION

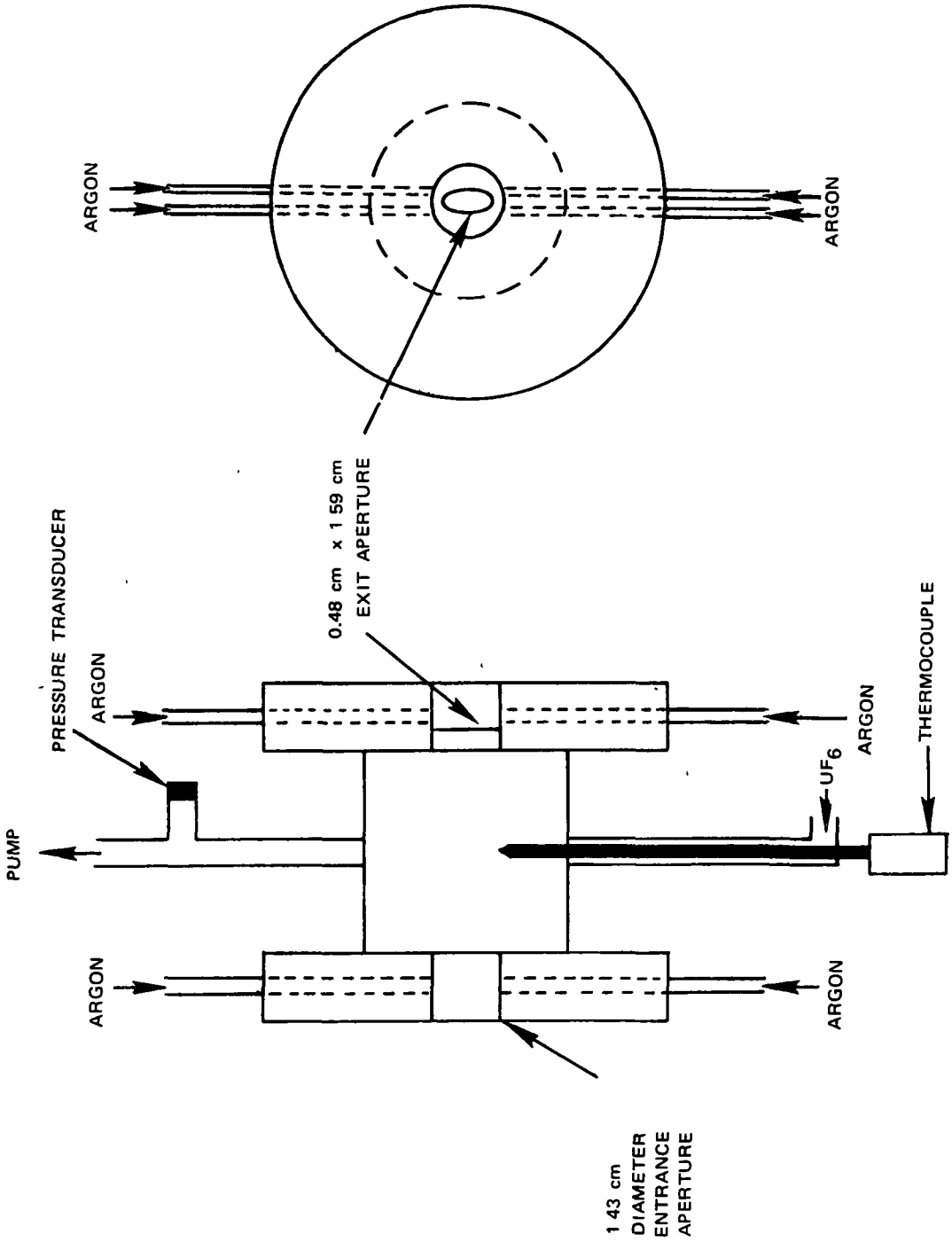

SODIUM SALICYLATE WINDOW ADAPTER

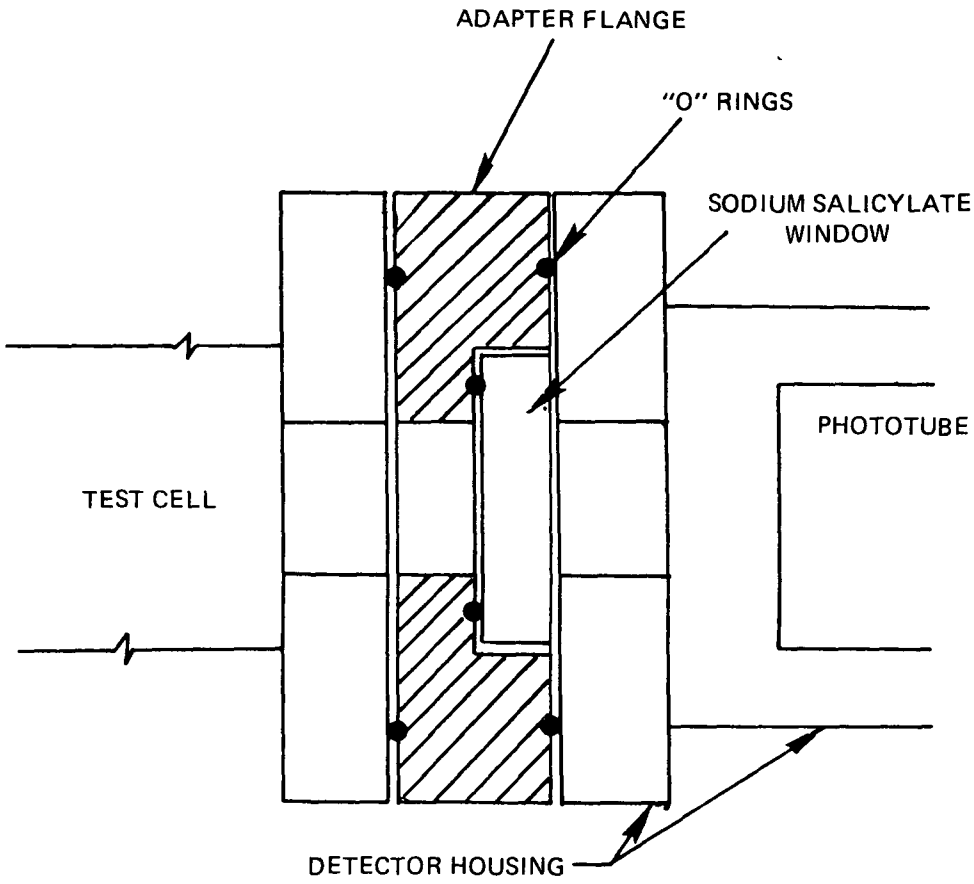

DIFFERENT SLIT ASSEMBLY MODIFICATION FOR HIGH PRESSURE OPERATION

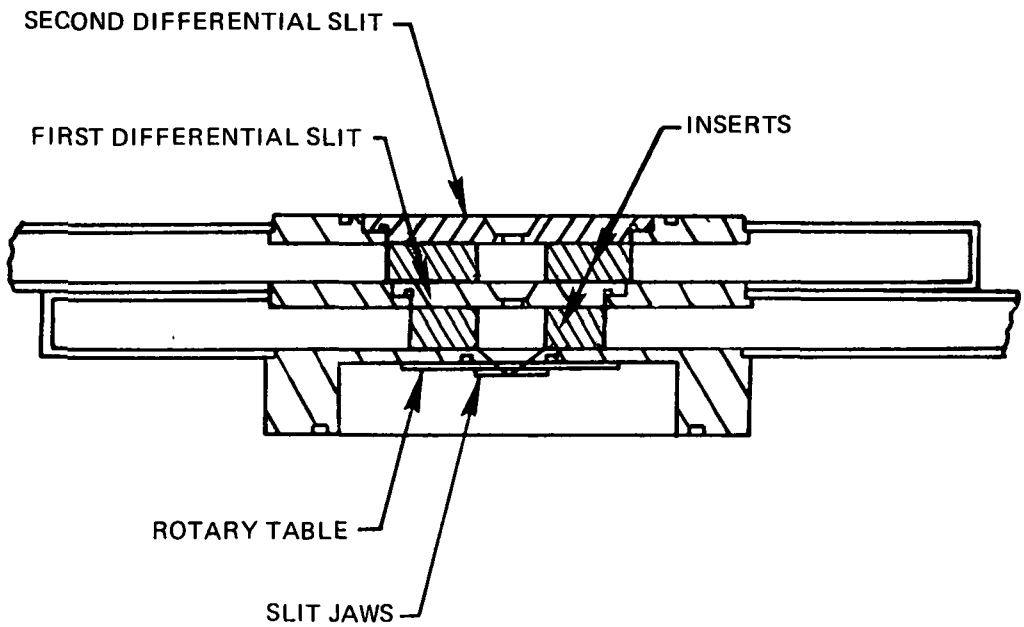

DIFFERENTIAL SLIT ASSEMBLY FLOW AND PRESSURE TEST CONFIGURATION

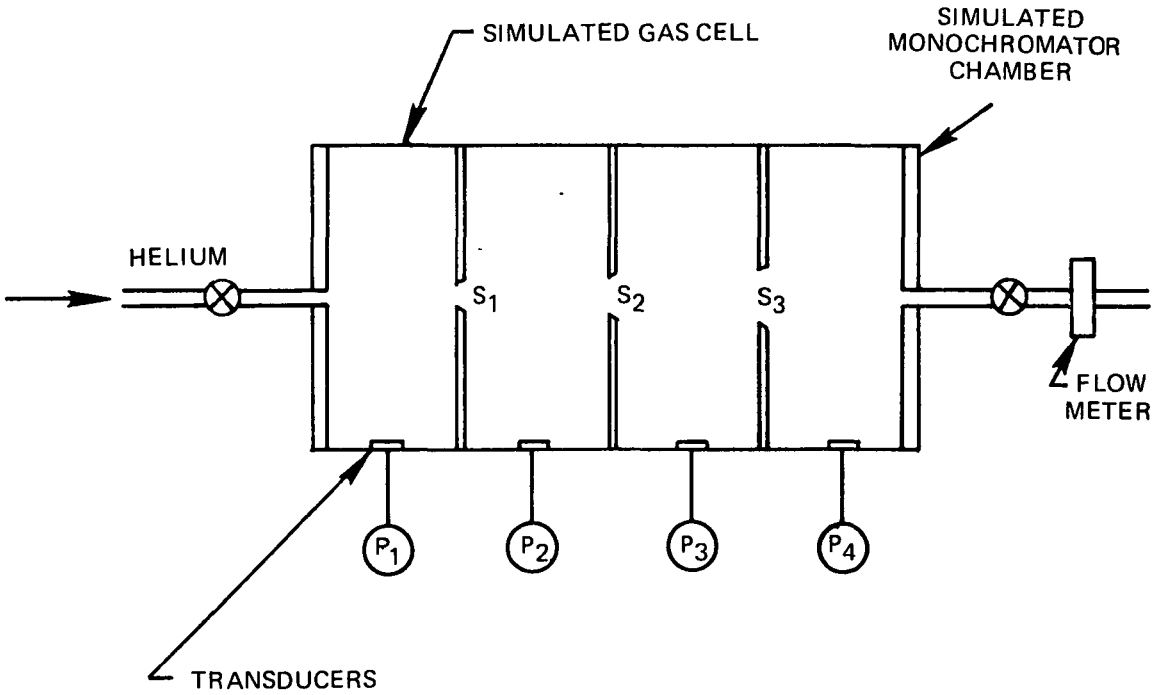

S_1 – VARIABLE WIDTH SLIT 10, 50 or 100 μ x 1.25 cm

S_2 – FIRST DIFFERENTIAL SLIT 0.183 cm x 0.498 cm

S_3 – SECOND DIFFERENTIAL SLIT. 0 351 cm x 0.584 cm

FIG. 22

COMPARISON OF HELIUM FLOW THROUGH VARIOUS SIZES OF DIFFERENTIAL SLITS, S_1, AS A FUNCTION OF PRESSURE, P_1

TEMPERATURE ≈ 300°K

SLIT HEIGHT = 1.27 CM

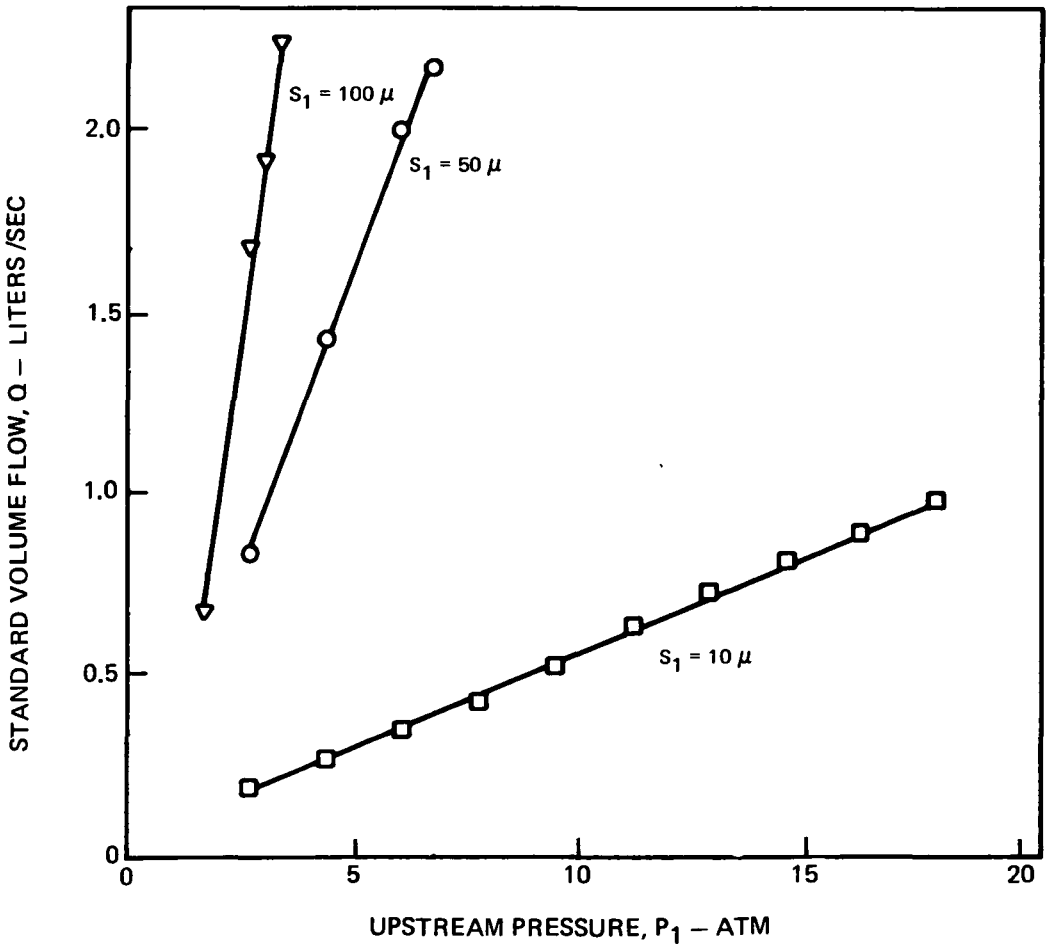

FIG. 23

RELATIVE SPECTRAL TRANSMISSION OF HELIUM BETWEEN 60 AND 110 NANOMETERS

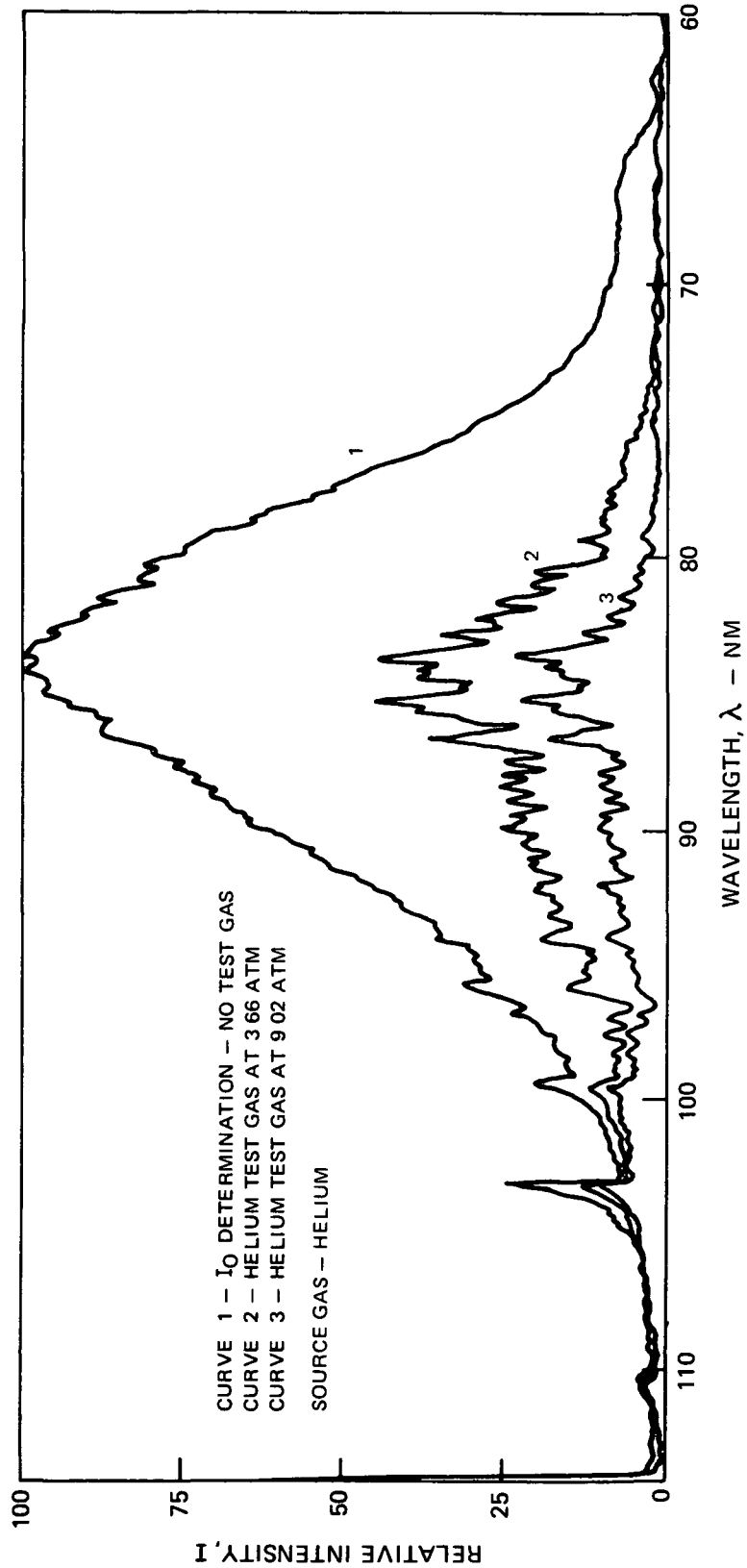

FIG. 24

RELATIVE SPECTRAL TRANSMISSION OF HELIUM BETWEEN 100 AND 160 NANOMETERS

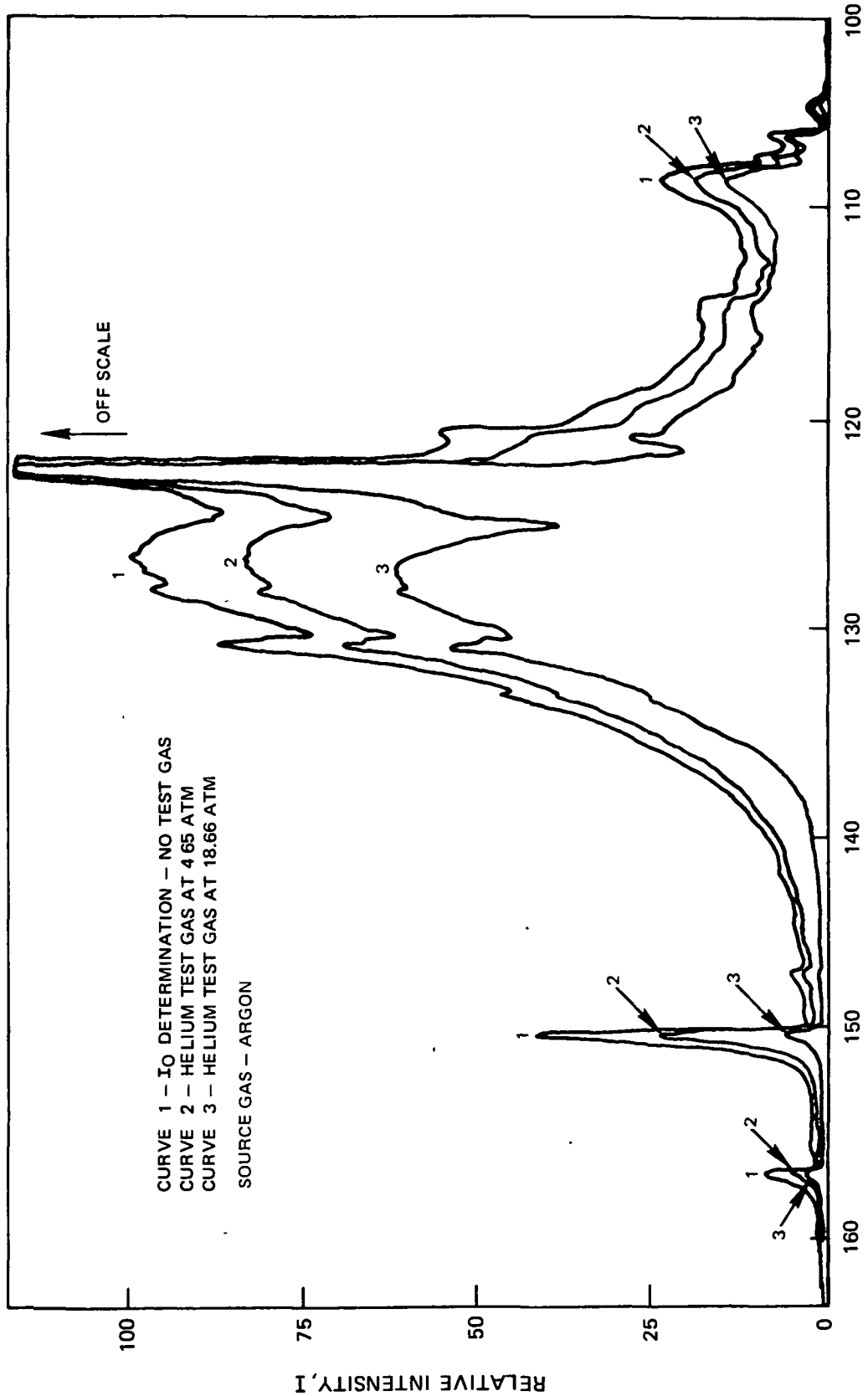

FIG. 25

RELATIVE SPECTRAL TRANSMISSION OF HELIUM BETWEEN 140 AND 200 NANOMETERS

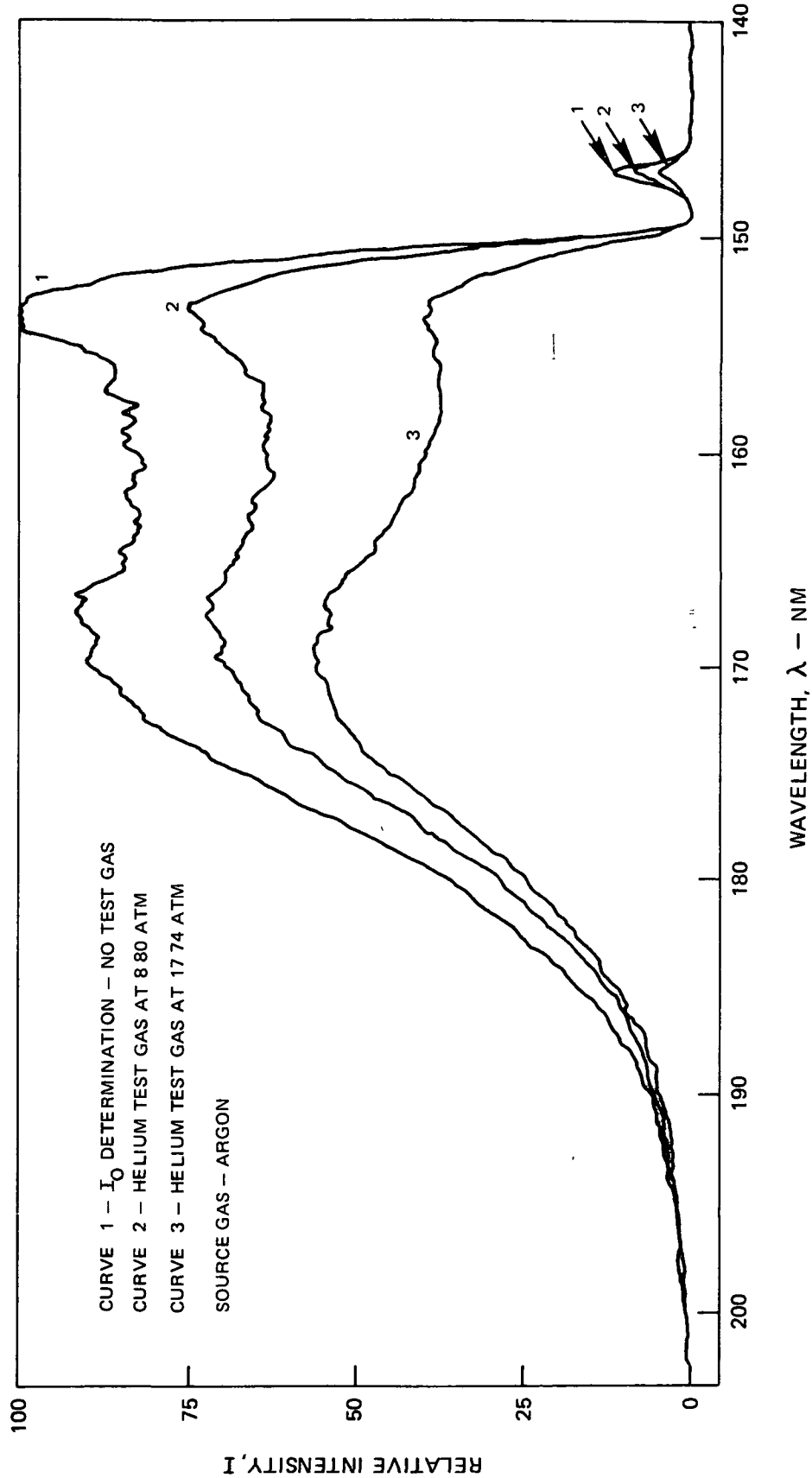

FIG. 26

RELATIVE SPECTRAL TRANSMISSION OF HELIUM BETWEEN 220 AND 300 NANOMETERS

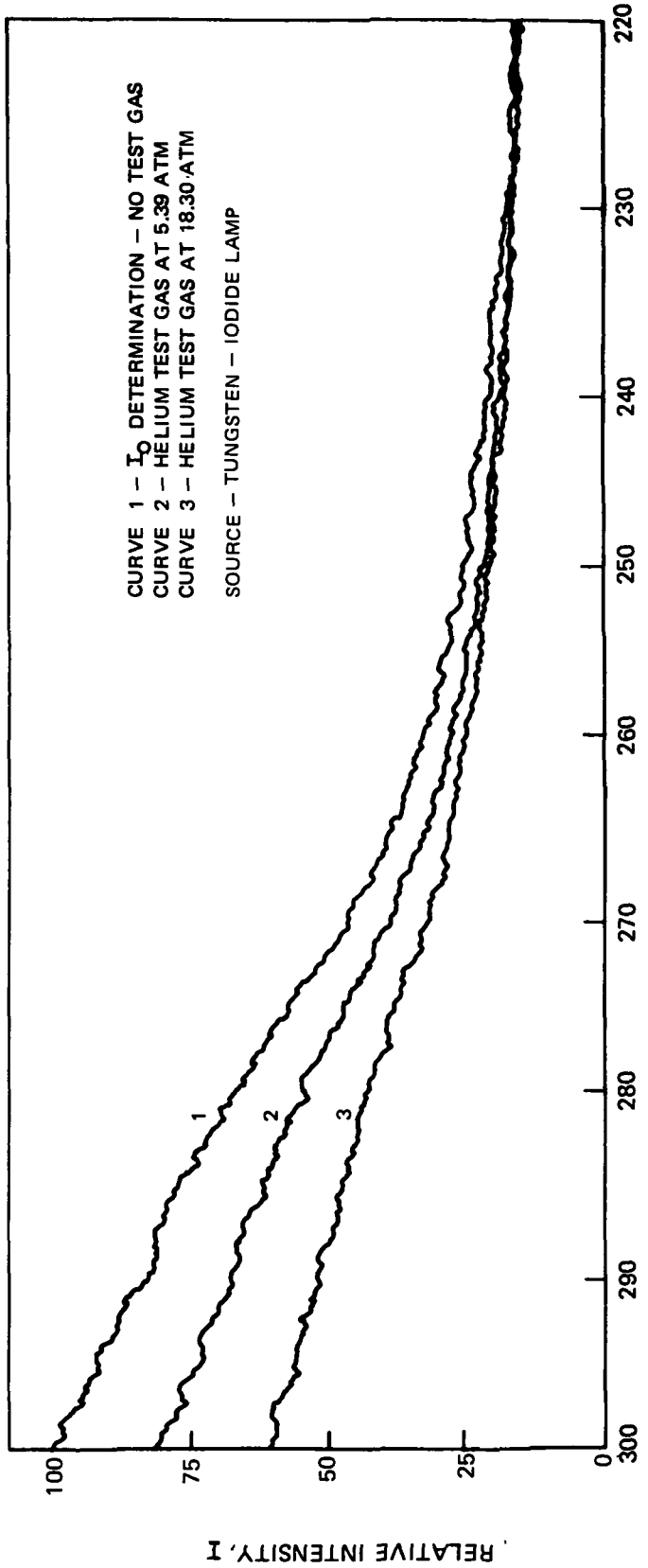

FIG. 27

RELATIVE SPECTRAL TRANSMISSION OF "CLEAN" HELIUM BETWEEN 60 AND 110 NANOMETERS

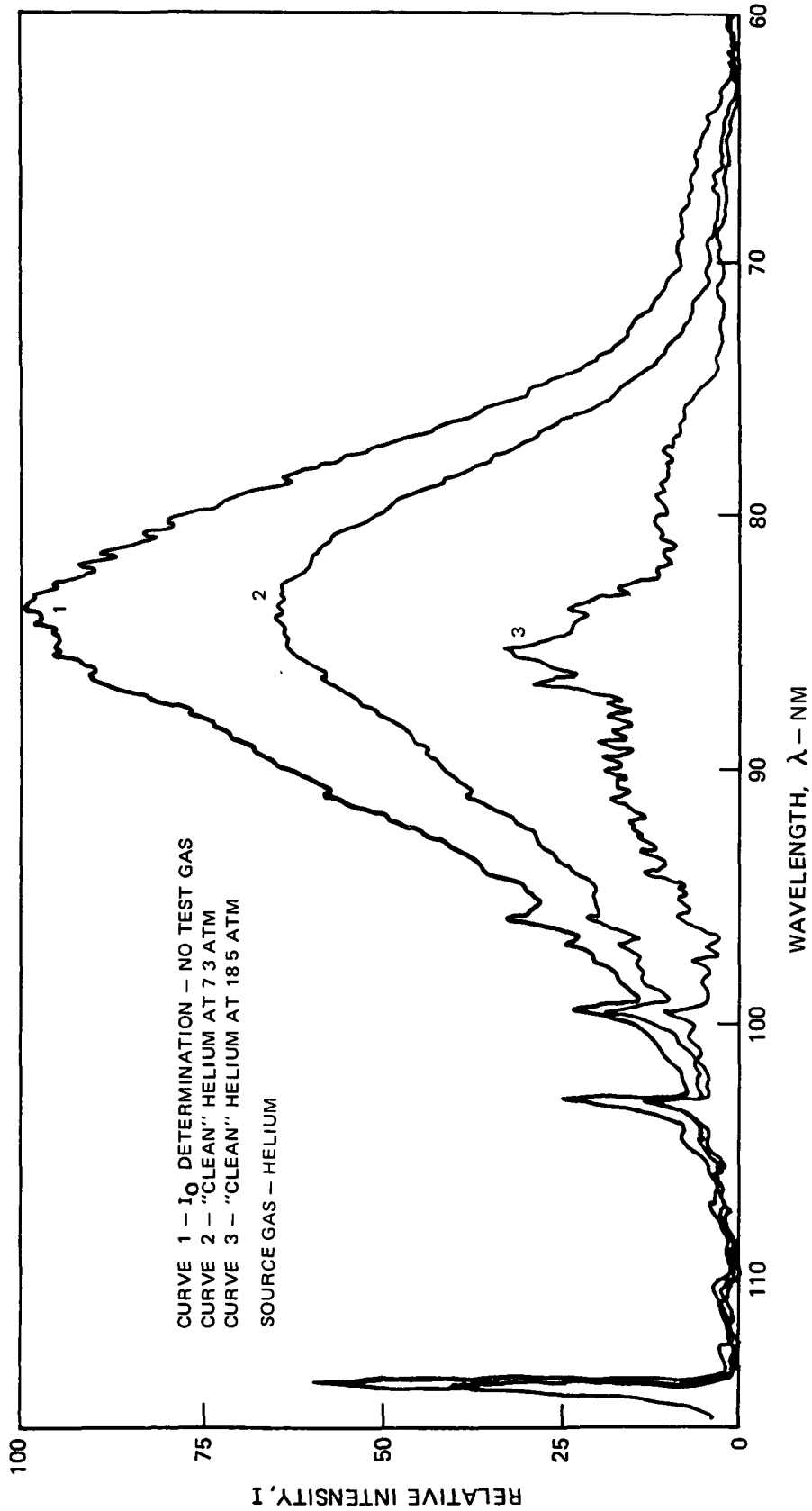

FIG. 28

RELATIVE SPECTRAL TRANSMISSION OF ARGON BETWEEN 60 AND 110 NANOMETERS

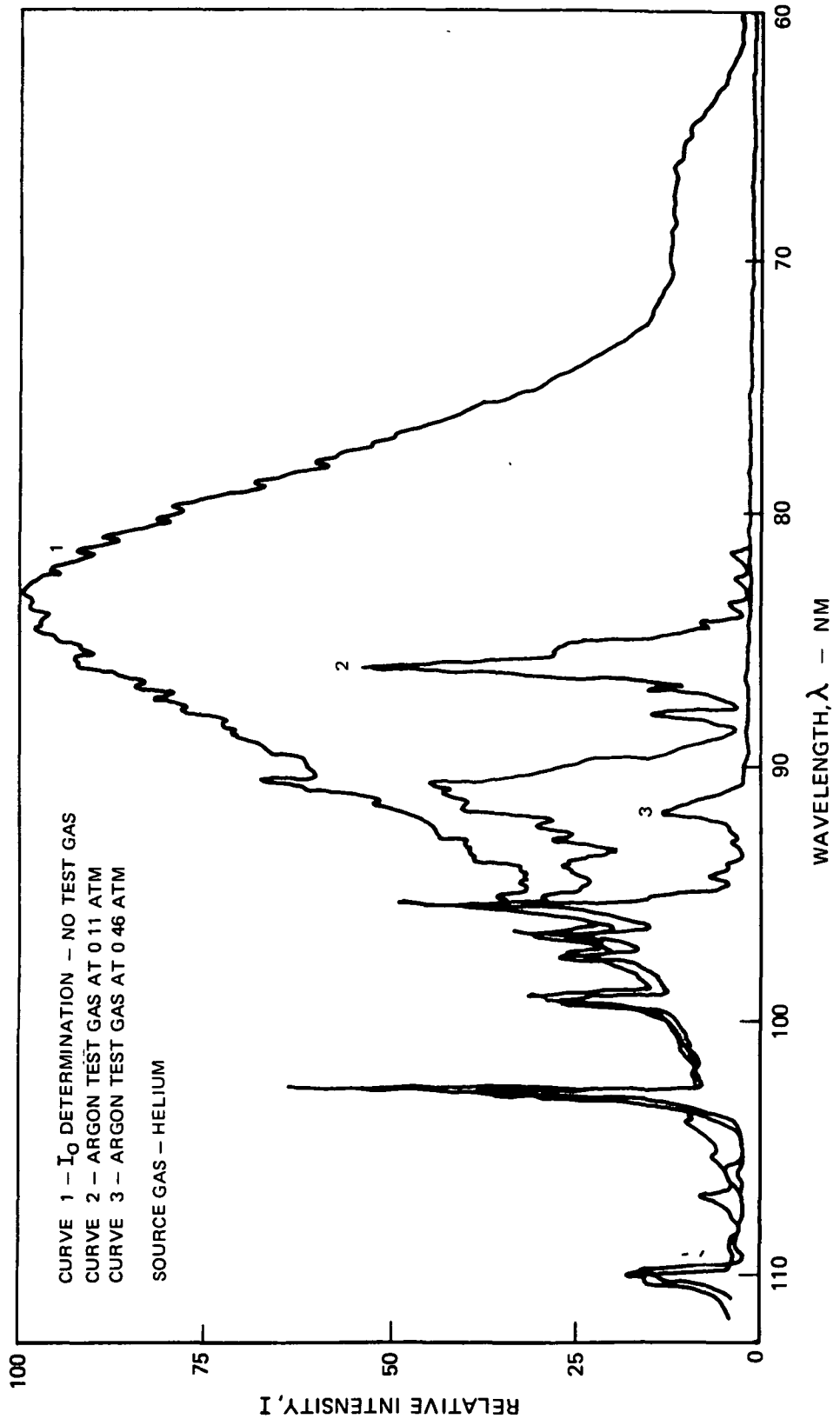

FIG. 29

RELATIVE SPECTRAL TRANSMISSION OF URANIUM HEXAFLUORIDE BETWEEN 60 AND 120 NANOMETERS

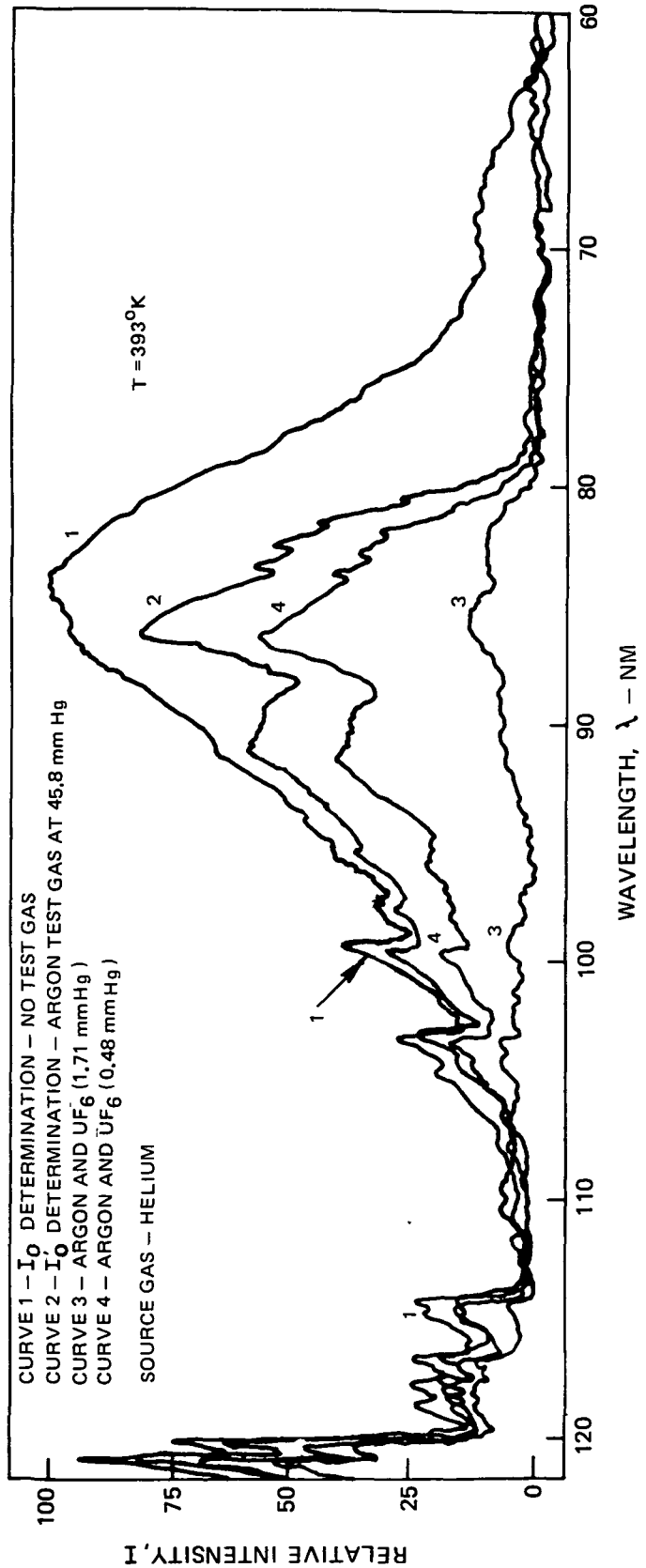

FIG. 30

RELATIVE SPECTRAL TRANSMISSION OF URANIUM HEXAFLUORIDE BETWEEN 120 AND 200 NANOMETERS

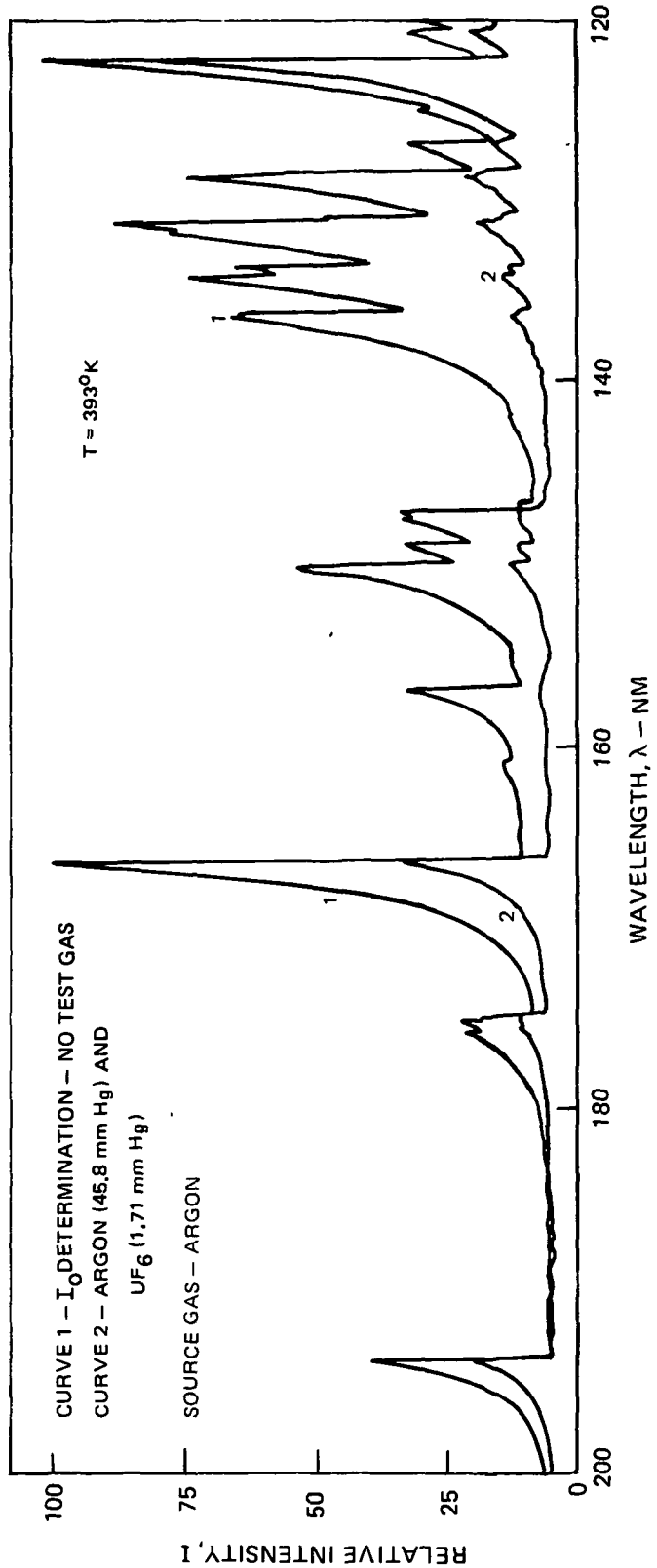

FIG. 31

SPECTRAL TRANSMISSION OF URANIUM HEXAFLUORIDE BETWEEN 80 AND 120 NANOMETERS

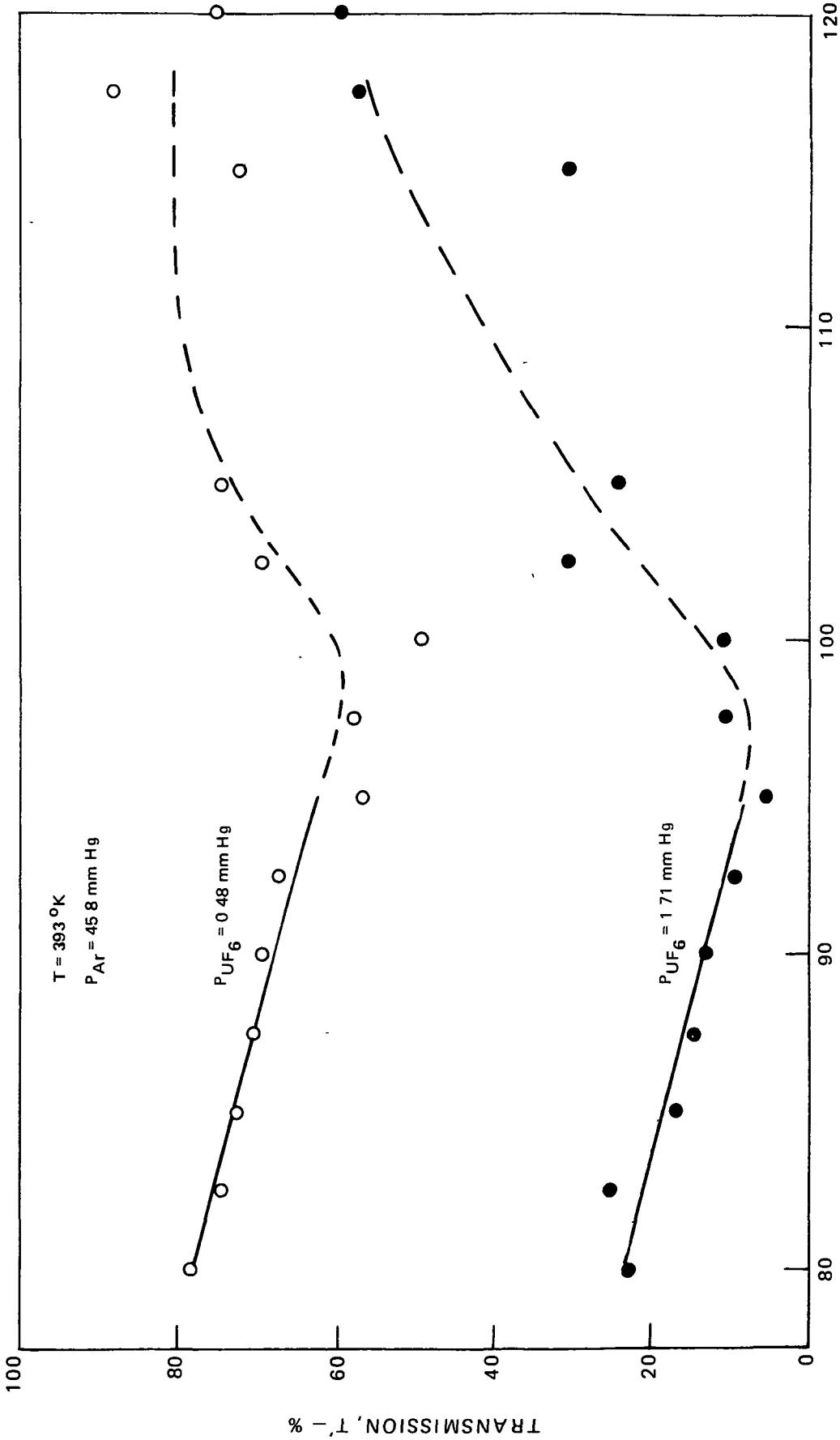

RO6–179–2

SPECTRAL TRANSMISSION OF URANIUM HEXAFLUORIDE BETWEEN 80 AND 100 NANOMETERS

$T' = I / I_o' \times 100$

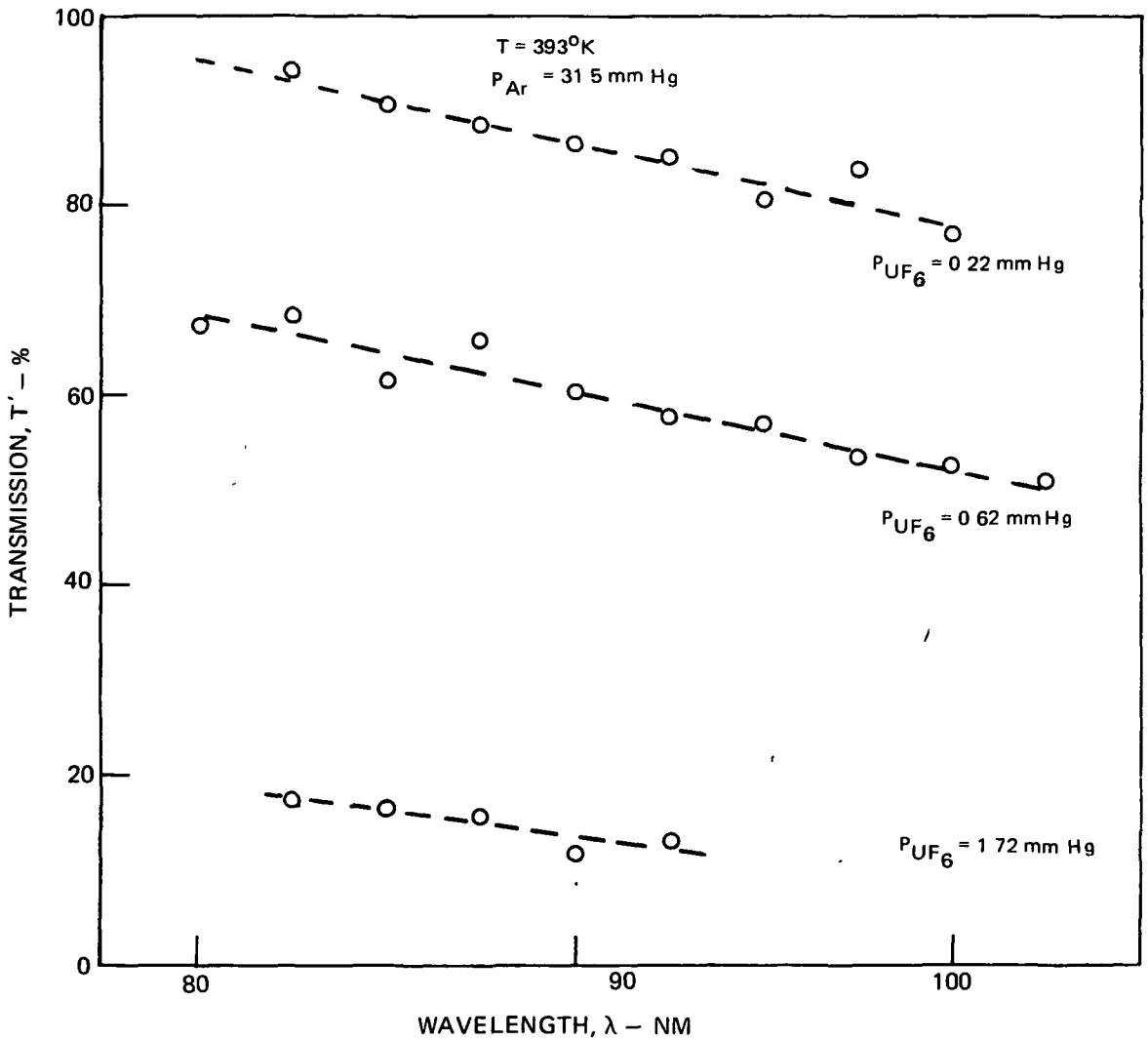

FIG. 33

ABSORPTION CROSS–SECTION OF URANIUM HEXAFLUORIDE BETWEEN 80 AND 120 NANOMETERS